Hybrid event beds dominated by transitional-flow facies: character, distribution and significance in the Maastrichtian Springar Formation, north-west Vøring Basin, Norwegian Sea

SARAH J. SOUTHERN*[1], IAN A. KANE†[2], MICHAŁ J. WARCHOŁ†,
KRISTIN W. PORTEN† and WILLIAM D. MCCAFFREY*
*Turbidites Research Group, School of Earth and Environment, University of Leeds, Leeds, LS2 9JT, UK (E-mail: s.southern88@gmail.com)
†Statoil ASA, Research Centre, Bergen NO-5020, Norway

Associate Editor – Peter Talling

ABSTRACT

Hybrid event beds comprising clay-poor and clay-rich sandstone are abundant in Maastrichtian-aged sandstones of the Springar Formation in the north-west Vøring Basin, Norwegian Sea. This study focuses on an interval, informally referred to as the Lower Sandstone, which has been penetrated in five wells that are distributed along a 140 km downstream transect. Systematic variations in bed style within this stratigraphic interval are used to infer variation in flow behaviour in relatively proximal and distal settings, although individual beds were not correlated. The Lower Sandstone shows an overall reduction in total thickness, bed amalgamation, sand to mud ratio and grain size in distal wells. Turbidites dominated by clay-poor sandstone are at their most common in relatively proximal wells, whereas hybrid event beds are at their most common in distal wells. Hybrid event beds typically comprise a basal clay-poor sandstone (non-stratified or stratified) overlain by banded sandstone, with clay-rich non-stratified sandstone at the bed top. The dominant type of clay-poor sandstone at the base of these beds varies spatially; non-stratified sandstone is thickest and most common proximally, whereas stratified sandstone becomes dominant in distal wells. Stratified and banded sandstone record progressive deposition of the hybrid event bed. Thus, the facies succession within hybrid event beds records the longitudinal heterogeneity of flow behaviour within the depositional boundary layer; this layer changed from non-cohesive at the front, through a region of transitional behaviour (fluctuating non-cohesive and cohesive flow), to cohesive behaviour at the rear. Spatial variation in the dominant type of clay-poor sandstone at the bed base suggests that the front of the flow remained non-cohesive, and evolved from high-concentration and turbulence-suppressed to increasingly turbulent flow; this is thought to occur in response to deposition and declining sediment fallout. This research may be applicable to other hybrid event bed prone systems, and emphasizes the dynamic nature of hybrid flows.

Keywords Clay-rich sandstone, hybrid event bed, hybrid flow, transitional flow, turbidite.

[1]Present address: Department of Geoscience, University of Calgary, Alberta T2N1R4, Canada.
[2]Present address: School of Earth, Atmospheric and Environmental Sciences, University of Manchester, Manchester M13 9PL, UK

INTRODUCTION

Deposits of flows transitional between turbidity current and debris flow

Sedimentological studies of the marginal and distal settings of deep-water distributive systems have increasingly documented sediment gravity flow deposits that comprise discrete clay-poor and clay-rich sandstone intervals within a single event bed (greywacke beds – Wood & Smith, 1958; slurry-flow deposits – Lowe & Guy, 2000; Sylvester & Lowe, 2004; linked debrites – Haughton *et al.*, 2003; co-genetic debrite–turbidite beds – Talling *et al.*, 2004; Amy & Talling, 2006; Barker *et al.*, 2008; hybrid event beds – Haughton *et al.*, 2009; Davis *et al.*, 2009; Hodgson, 2009; low-strength and intermediate-strength cohesive debris flow deposits – Talling *et al.*, 2010, 2012a; transitional flow deposits – Kane & Pontén, 2012). Many of these studies show, or infer, a spatial change in deposit character from clay-poor sandstone beds, i.e. classical turbidites, to beds containing clay-poor and clay-rich sandstones in downstream (proximal to distal) or across-flow (axial to marginal) directions. This facies tract is considered to record transformation of a flow event with non-cohesive behaviour, to a flow event in which a cohesive turbulence-suppressed behaviour became more significant: occurring either at a region in the rear of the flow (Haughton *et al.*, 2009) or more extensively across the flow (e.g. Talling *et al.*, 2007). Such variation is typically expressed over several kilometres or more (i.e. Haughton *et al.*, 2003, 2009; Hodgson, 2009; Davis *et al.*, 2009; Talling *et al.*, 2012a); variation over shorter length-scales (tens to hundreds of metres) has been recognized and is attributed to scenarios promoting a more rapid change in flow parameters (e.g. Terlaky & Arnott, 2014; Fonnesu *et al.*, 2015). The increased significance of cohesive flow behaviour during run-out differs from the classic model for fluidal sediment gravity flows (i.e. turbidity currents), which involves increasing turbulence and differential grain settling in response to declining sediment concentration via progressive deposition of sediment and entrainment of ambient fluid (Bouma, 1962; Lowe, 1982; Mutti, 1992; Mulder & Alexander, 2001; Stow *et al.*, 1996).

Sediment gravity flow behaviour can be modified by changes in the concentration and relative proportions of clastic material (e.g. grain size and type, Lowe, 1982; Lowe & Guy, 2000; Mulder & Alexander, 2001; Baas & Best, 2002; Baas *et al.*, 2009, 2011; Sumner *et al.*, 2009; Manica, 2012). Downstream change to a more cohesive behaviour results from an increasing proportion of clay and electrostatic bonding of clay particles within the flow, and is promoted by: (i) clay enrichment by partial to total loss (deposition) of coarse sand fractions (Wood & Smith, 1958; Talling *et al.*, 2004; Barker *et al.*, 2008; Sumner *et al.*, 2009); (ii) clay enrichment due to entrainment of muddy substrate (Ricci Lucchi & Valmori, 1980; Haughton *et al.*, 2003, 2009); or (iii) deceleration and reduction in shear and fluid turbulence, which otherwise prevent cohesive bonding within clay-rich flow (Talling *et al.*, 2007; Baas *et al.*, 2009, 2011; Sumner *et al.*, 2009). Experimental studies have demonstrated how relatively small increases in clay concentration can drive significant changes in flow behaviour, as well as how sediment is supported and deposited (Baas & Best, 2002; Baas *et al.*, 2005, 2011; Sumner *et al.*, 2009).

Haughton *et al.* (2009) proposed the term hybrid event bed for deposits that record deposition 'at a fixed point' from non-cohesive to cohesive flow behaviour during the passage of a single sediment gravity flow. Such sediment gravity flows are interpreted to have evolved from non-cohesive flow behaviour, to a flow that was longitudinally partitioned into discrete rheological zones, with non-cohesive behaviour at the front and cohesive behaviour at the rear (i.e. hybrid flow *sensu* Haughton *et al.* 2009). The rearward transitions in flow behaviour are suggested to either be: (i) progressive where banded sandstones record transient fluctuating non-cohesive and cohesive behaviour (i.e. slurry flow – Lowe & Guy, 2000; transitional flow – Baas *et al.*, 2005; Haughton *et al.*, 2009); or (ii) more abrupt where banded sandstones are absent (Haughton *et al.*, 2009). Where indicators of progressive aggradation of the bed beneath a passing flow are lacking (i.e. banding or lamination), the origin of the clay-poor sandstone at the base of the bed is ambiguous. It may record high sediment fall-out rates from non-cohesive flow, or late-stage sand settling from a low-yield strength cohesive flow incapable of supporting the coarsest sand fractions (Marr *et al.*, 2001; Mohrig & Marr, 2003; Talling *et al.*, 2004, 2012a; Sumner *et al.*, 2009).

Inferring sediment gravity flow behaviour from their deposits

Many studies have used the deposits of sediment gravity flows to infer flow character and evolution. Predictions of flow behaviour are of higher confidence where individual beds can be correlated over relatively long distances. However, such instances are rare (e.g. Amy & Talling, 2006; Talling *et al.*, 2007, 2012a; Stevenson *et al.*, 2014). Furthermore, it should be noted that even facies tracts within individual beds are themselves likely to be diachronously deposited and represent different parts of flows that evolved spatially and temporally (e.g. axis and off-axis positions within a sediment gravity flow, Barker *et al.*, 2008). Inferring longitudinal flow processes from typical bed characteristics within a wider stratigraphic interval entails greater uncertainty, because beds representing multiple different types of flow event (e.g. Talling *et al.*, 2012a) could be grouped and jointly interpreted. Nevertheless, this approach has been adopted in many highly influential process-based models of deepwater sedimentation (e.g. Lowe, 1982; Mutti, 1992; Lowe & Guy, 2000; Haughton *et al.*, 2003, 2009) and can be justified as a viable approach in subsurface studies, given the difficulties in establishing bed-scale correlations.

A range of sediment gravity flow deposits, including hybrid event beds, are present in sandstones of the Maastrichtian Springar Formation of the north-west Vøring Basin. Five cored wells that penetrate parts of a major sand-rich fairway are documented, with the aim of answering the following questions: (i) What is the spatial distribution of bed types? (ii) How do stratigraphic stacking patterns compare with spatial bed type distributions? (iii) Do bed type distributions provide insight for the development of process-based models for facies distribution? (iv) What factors influence the development of hybrid event bed facies and why are they common in some systems but not others? (v) What are the implications for the prediction of depositional environment and of reservoir quality?

GEOLOGICAL SETTING

Basin setting

The Vøring Basin is located 300 km west of Mid-Norway in the Norwegian Sea. It formed during two regionally extensive rifting episodes of late Jurassic to early Cretaceous and late Cretaceous to Palaeocene age, which resulted in the opening of the Atlantic Ocean (Skogseid & Eldholm, 1989; Roberts *et al.*, 1997; Færseth & Lien, 2002; Fjellanger *et al.*, 2005) (Fig. 1A and B). Late Cretaceous rifting was accompanied by deposition of marine mudstone-dominated successions that contained deep-water sandstone accumulations (Kvitnos, Nise and Springar formations – Kittilsen *et al.*, 1999; Færseth & Lien, 2002; Lien *et al.*, 2006). This study focuses on Maastrichtian-aged deep-water sandstones (Hvithval Member) of the Springar Formation, which accumulated during rifting and an overall relative sea-level rise (Surlyk, 1990; Riis, 1996). Uplift and erosion of the East Greenland Margin provided a siliciclastic supply to the Vøring Basin during the Late Cretaceous (Fonneland *et al.*, 2004; Morton *et al.*, 2005) (Fig. 1B). Sediments were transported eastward across the developing 'proto' Gjallar Ridge (Lundin & Doré, 1997; Færseth & Lien, 2002; Roberts *et al.*, 2009), into the deeper part of the basin in the Vigrid Syncline area (Færseth & Lien, 2002; Lien *et al.*, 2006); sediment delivery into the deeper basin was permitted by structural lineaments that dissected the ridge (Fjellanger *et al.*, 2005). Uplift of the Gjallar Ridge commenced in the Campanian, and continued piecemeal into the Tertiary (Lundin & Doré, 1997; Roberts *et al.*, 2009), with significant erosion occurring along the ridge towards the end of the Cretaceous (Lundin *et al.*, 2013; Fjellanger *et al.*, 2005). Maastrichtian-aged deep-water sandstones were emplaced by sediment gravity flows, and comprise very fine-grained to medium-grained sandstone of sub-arkosic composition, with detrital clay content ranging from 2 to 26% (Porten *et al.*, 2016).

Stratigraphic framework

Three distinct Maastrichtian-aged sandstone intervals are recognized, which are informally referred to as the Lower, Middle and Upper Sandstone (Fig. 2). The sandstone intervals were identified based on the thick mudstone-dominated succession in Well 1 (*ca* 2850 m), and biostratigraphic analyses that employ an in-house biozonation scheme based on palynology and micropalaeontology. The Upper Sandstone is only present in Well 2 and implies that siliciclastic deposition was limited in extent or was offset with respect to Wells 3 to
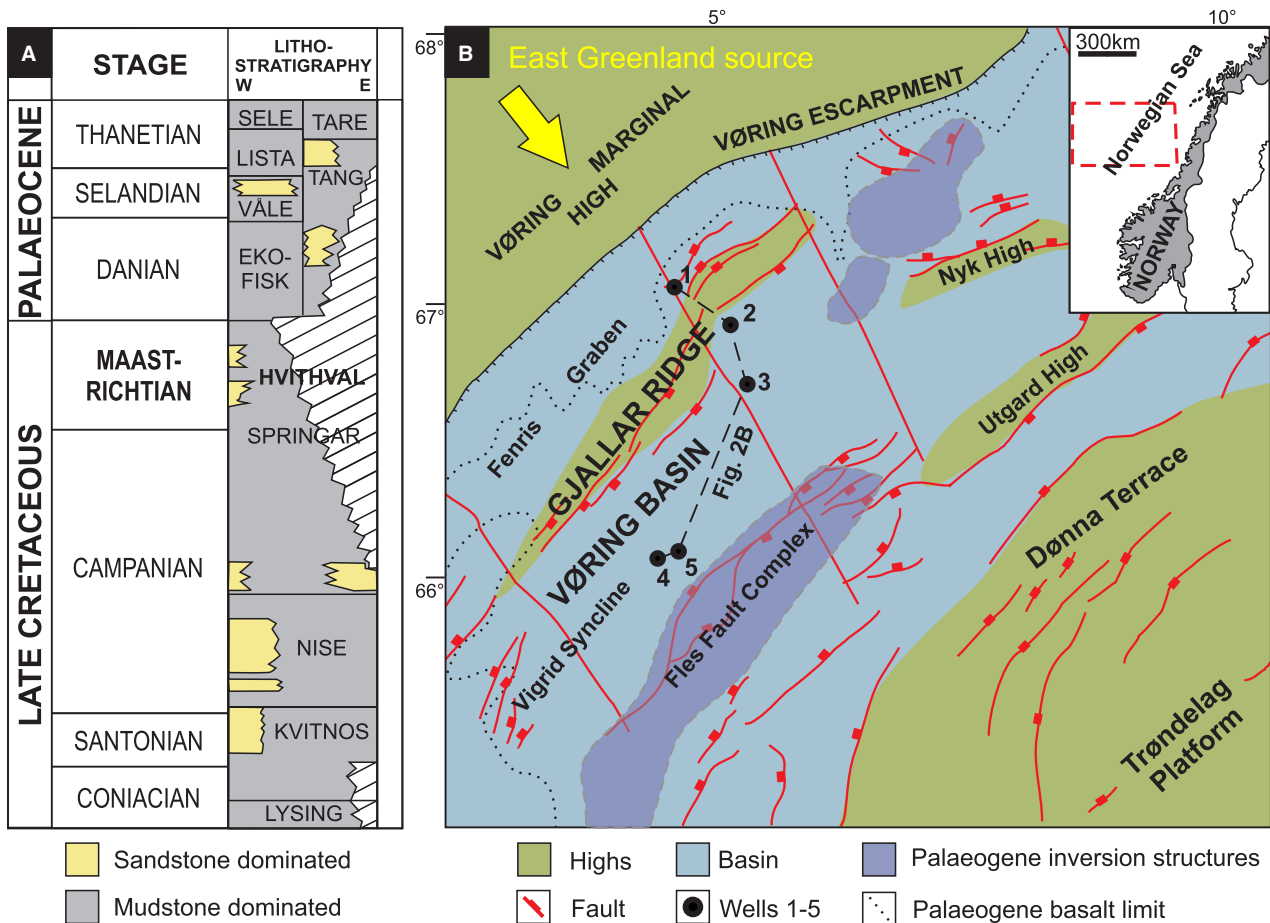
Fig. 1. Late Cretaceous to Palaeocene stratigraphic column (A) and palaeogeographic map (B) of the Vøring Basin showing the location of studied wells. Well 1 (6704/12-1), Well 2 (6705/10-1), Well 3 (6605/1-1), Well 4 (6604/10-1) and Well 5 (6603/12-1). Modified from Færseth & Lien (2002).

5; its absence in Well 1 is attributed to pre-Danian erosion in the Gjallar Ridge area. The Middle Sandstone only occurs in Well 1, implying that siliciclastic sediments were largely retained behind the ridge at this time, and that any deposition in the deeper basin was offset with respect to the other wells. The Lower Sandstone interval occurs in all five wells and is the focus of this study. The total thickness of the Lower Sandstone decreases in distal settings (Wells 4 and 5); its limited thickness in Well 2 is attributed to post-depositional modification (remobilization or erosion) in the Gjallar Ridge area, and is discussed further below. Seismic reflection data demonstrates the age correlation of the Lower Sandstone within the early Maastrichtian interval (Fig. 2), and an overall elongation of sandstone accumulations from north to south. However, the limited resolution of the seismic data and erosion along

the Gjallar Ridge precludes well-constrained correlations of the Lower Sandstone between all studied wells.

DATA AND METHODS

Five exploration wells that penetrate sandstones of the Hvithval Member of the Springar Formation form the basis of this study; these are distributed along a *ca* 140 km proximal to distal transect from the Gjallar Ridge area to the Vigrid Syncline that represents the deeper part of the basin (Figs 1, 2 and 3). The Lower Sandstone (LS) is penetrated by all five wells from which 121·5 m of core has been described in terms of lithology, grain size, sorting and sedimentary structures (Figs 1, 2 and 3). Point counting of thin-sectioned core samples provided the texture and compositional data for
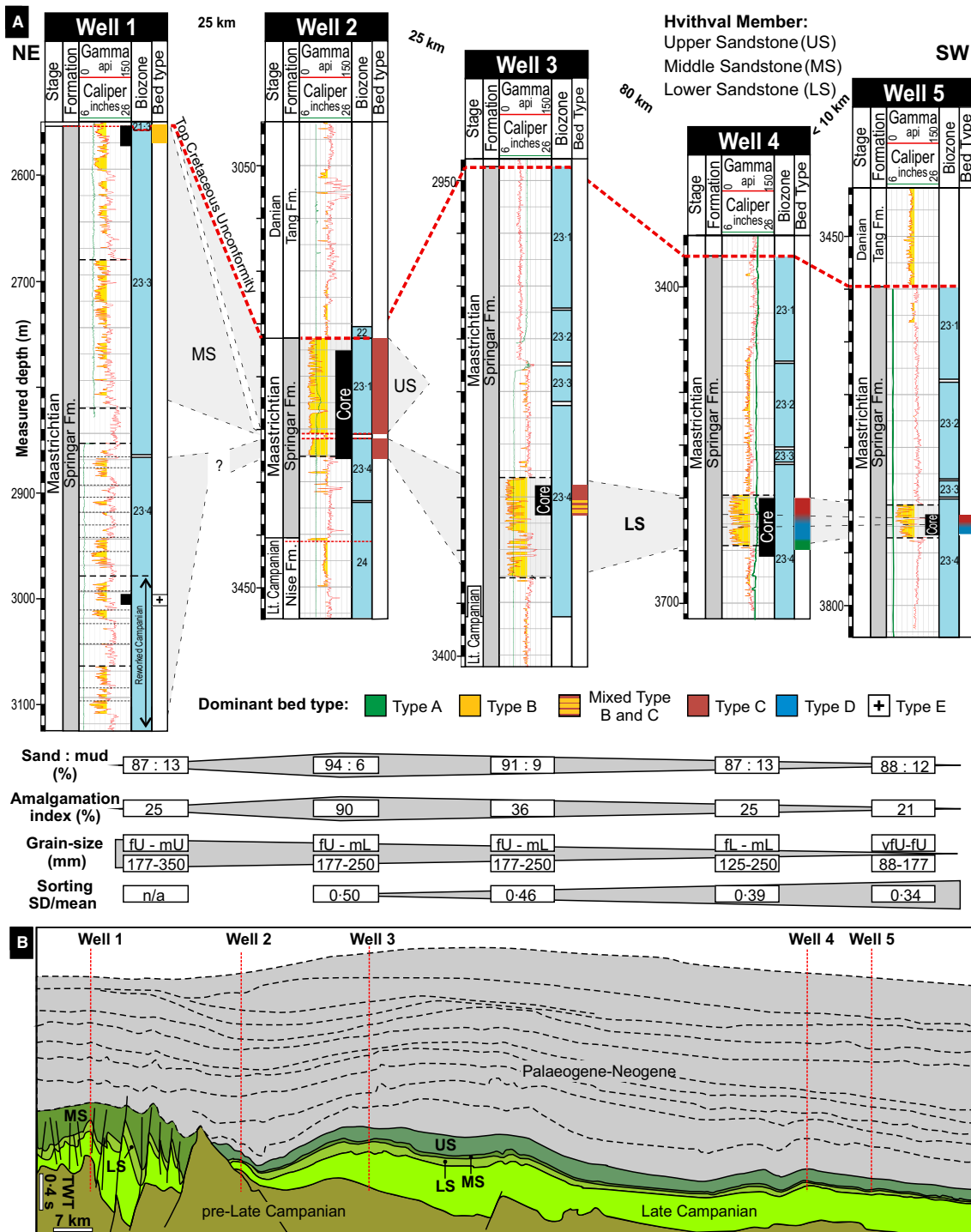
Fig. 2. (A) Summary of the five exploration wells that penetrate Maastrichtian-aged sandstones within the Springar Formation. Three distinctly aged sandstone packages are highlighted by biostratigraphy (microfossil and palynological data) and thick bounding mudstones (i.e. *ca* 2800 m, Well 1). The extensively occurring Lower Sandstone forms the basis of this study; sedimentological characteristics were determined using core from this interval, with the amalgamation ratio value determined *sensu* Romans *et al.* (2009). See Fig. 1 for well locations. (B) Schematic interpreted seismic section showing the location of wells with respect to the Gjallar Ridge, and the broad age correlation of early Maastrichtian-aged strata containing the Lower Sandstone (LS). Uplift of the Gjallar Ridge occurred piecemeal during the Late Cretaceous – Palaeocene (Lundin & Doré, 1997; Roberts *et al.*, 2009). Original seismic data are not permitted for publication.
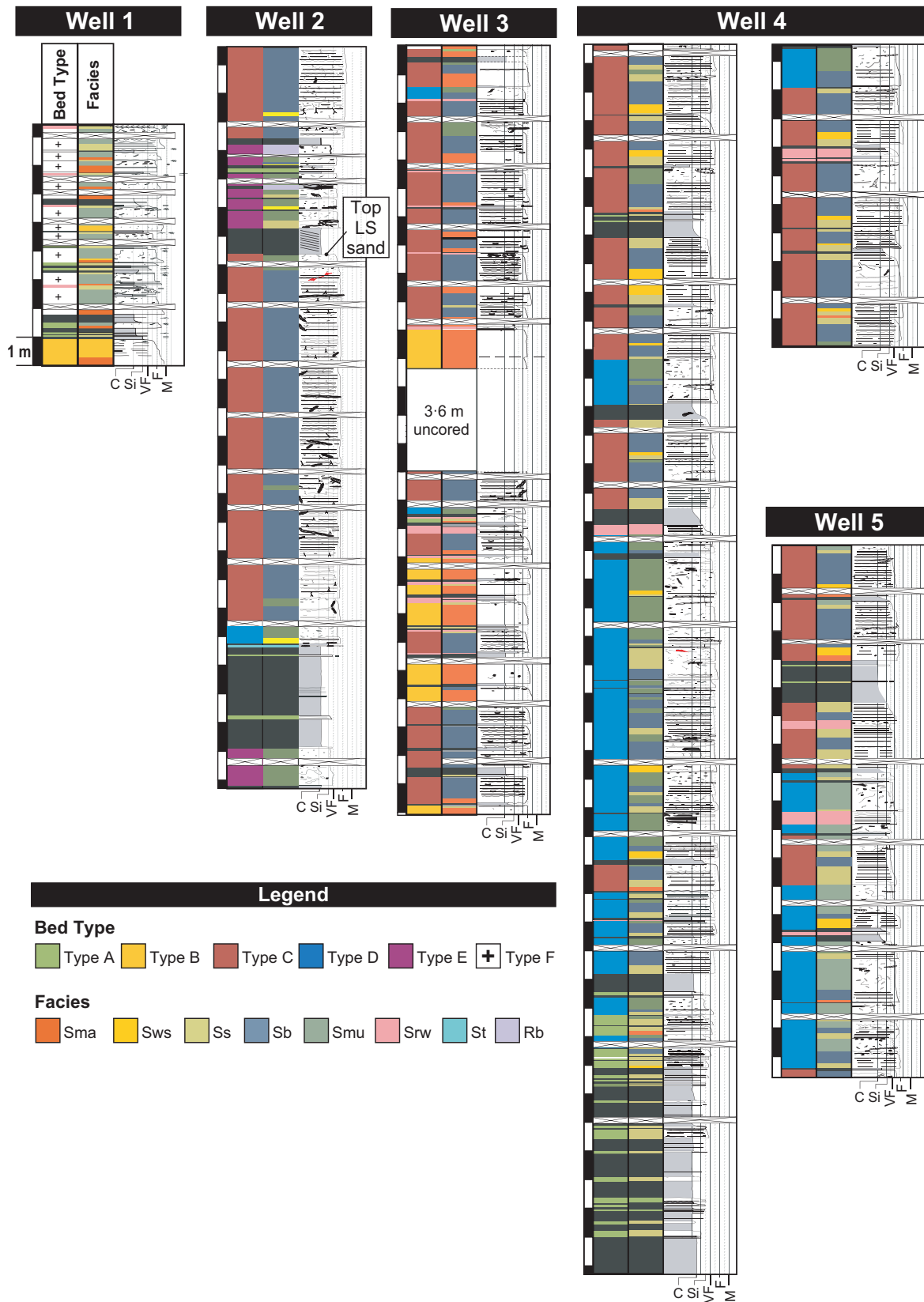
Fig. 3. Graphic sedimentary logs illustrating facies and bed type occurrence within Lower Sandstone (LS) of Wells 1 to 5: C = clay; Si = Silt; VF = very fine sand; F = fine sand; M = medium sand.

sandstone facies. The proportion and occurrence of bed types, and their constituent facies, were recorded in order to gain insight into spatial (stratigraphic and downstream) variations in associated depositional processes. Wireline logs did not facilitate correlation of smaller scale packages within the LS, but provided some insight into non-cored parts of the stratigraphy.

FACIES AND BED TYPES OF THE LOWER SANDSTONE

Sandstone facies are defined based on sediment composition, texture and sedimentary structures (Fig. 4; Table 1). Bed types were defined based on the type and proportion of their constituent sandstone facies (Figs 5 and 6). The descriptive and interpretative terminology of facies and bed
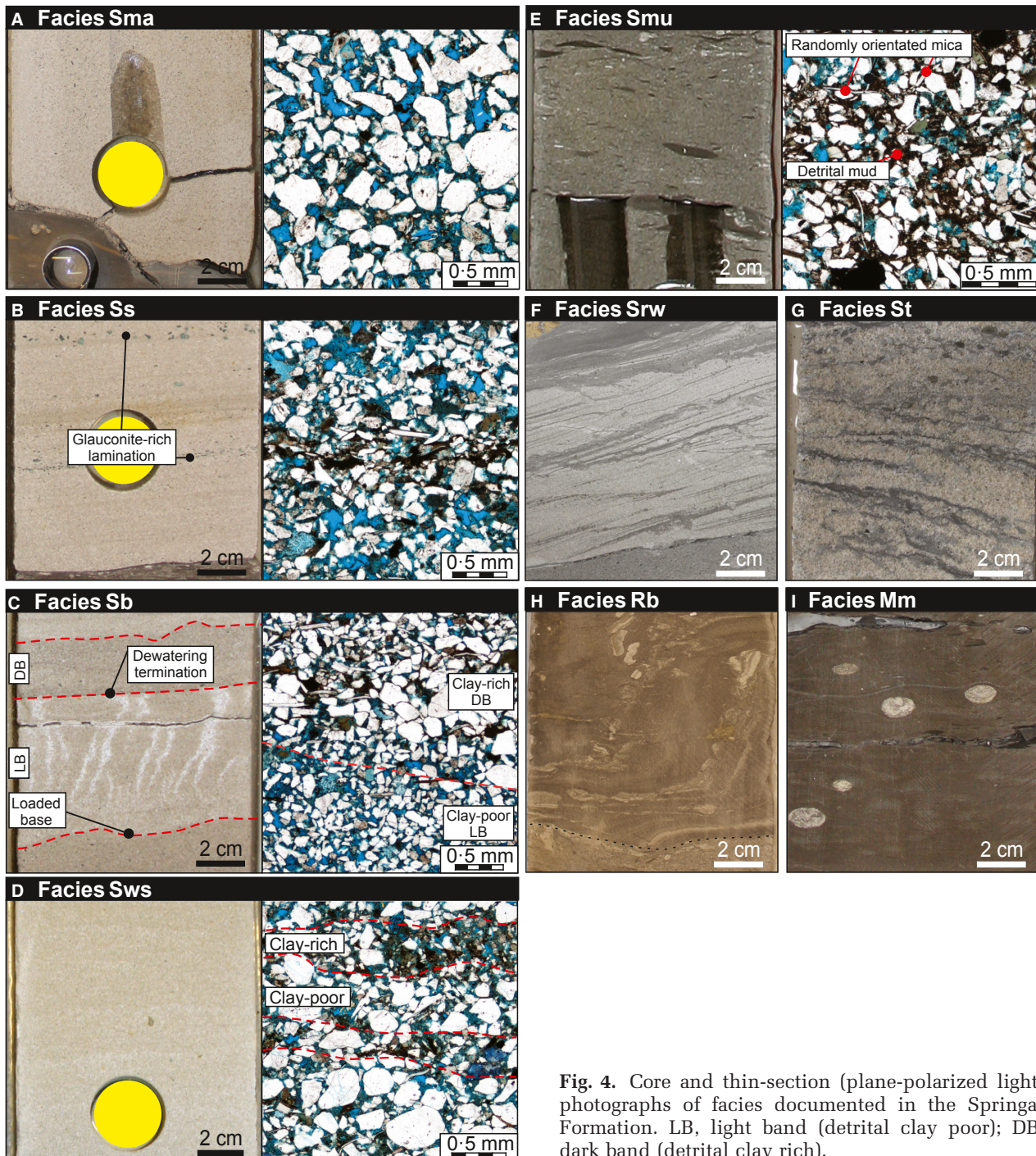

Fig. 4. Core and thin-section (plane-polarized light) photographs of facies documented in the Springar Formation. LB, light band (detrital clay poor); DB, dark band (detrital clay rich).

Table 1. Description and process interpretation for facies present within the Springar Formation.

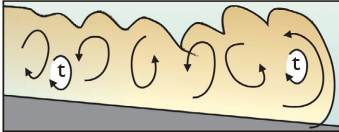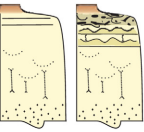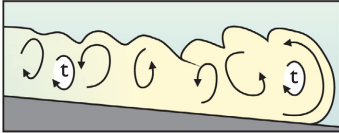| Facies	Colour	Grain size (μm) and sorting	Grading	Detrital clay (%)	Position	Structures	Interpretation
Sma Non-stratified sandstone	Medium – pale grey	fL–mU (125 to 375); Moderate–poor	Weak normal or ungraded	4·0% to 7·0%, 5·3% average	Lower bed; proximal	Non-stratified relatively clean sand that sometimes contains mud-clasts aligned on horizons parallel to bedding	(i) Rapid suspension fallout from high density turbidity current (Middleton, 1967; Lowe, 1982. Arnott & Hand, 1989). (ii) En masse freezing of sand-rich flow (Allen, 1991). (iii) Progressive aggradation beneath sustained turbidity current (Kneller & Branney, 1995)
Ss Stratified sandstone	Medium grey – beige	vfU–mU (94 to 375); Moderate	Normal	4·3% to 9·0%, 6·3% average	Lower–upper bed; distal	Relatively clean sand with planar-parallel to wavy laminae (<5 mm) and rarer ripple-cross-lamination. Laminae often lined with glauconite grains and rare mud-clasts	Deposition beneath a tractional flow boundary zone below a dilute turbulent flow in lower to upper flow regimes (Allen, 1984, Best & Bridge, 1992)
Sws Weakly stratified sandstone	Medium – pale grey	fL–mL (125 to 250); Moderate–poor	Normal	4·6% to 9·3%, 7·0% average	Lower bed; proximal–distal	Faint colour banding with darker bands being slightly more clay-rich and finer-grained. Characteristics similar to both facies Ss and Sb	Flow character that is transitional between flow states responsible for the emplacement of facies Ss and Sb
Sb Banded sandstone	Medium grey – beige	fL–mU (125 to 375); Moderate	Weak normal or ungraded	5·3% to 9·3%, 7·3% average	Lower–upper bed; proximal–distal	Colour-banded sand with dark bands richer in detrital clay, mica and organics with relatively poorer sorting. Pale bands load into dark bands. Dewatering pipes and dishes are abundant and often pervasive	(i) Temporal fluctuation of near-bed flow clay concentration driven by cycles of poor and improved fluid turbulence, thus sediment mixing (Lowe & Guy, 2000; Baas et al., 2005); (ii) reworking beneath turbulence enhanced transitional flow (Baas et al., 2011)
Smu Clay-rich Non-stratified sandstone	Medium – dark grey	fL–fU (125 to 250); Moderate–poor	Ungraded – weak normal	8·0% to 26·0%, 12·0% average	Upper bed; distal	Matrix-supported mud-rich sand that may contain mud-clasts typically 0·1 to 8·0 cm and sub-rounded. Clast alignment may be random or crudely bed-parallel	En masse deposition from a cohesive, turbulence suppressed flow with varying degrees of cohesive strength suggested by clast alignments (Major, 1997; Talling, 2013)
Srw Complex stratified sandstone	Pale – medium grey	vfU–mL (94 to 250); Moderate – well	Normal – inverse	No data	Isolated beds or bed-top; proximal–distal	Sharp tops, mud drapes; opposing current direction indicators; internal scouring; sharp grain-size contrasts with underlying facies	Depositional product of reworking and deposition by bottom currents (Sanders, 1965; Hubert, 1964; Lovell & Stow, 1981)
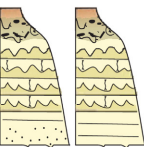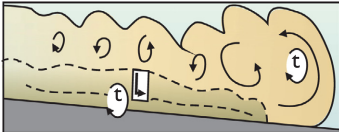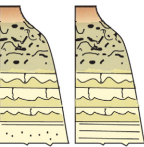
Table 1. (continued)

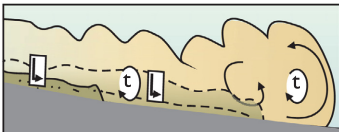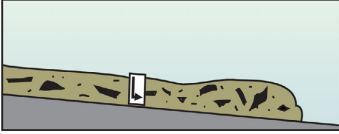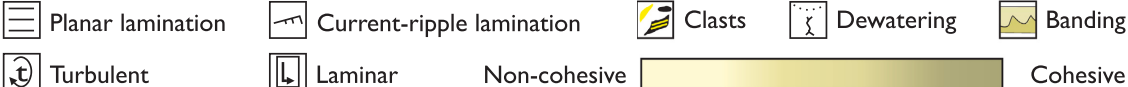| Facies	Colour	Grain size (μm) and sorting	Grading	Detrital clay (%)	Position	Structures	Interpretation
St Mud-clast-rich. weakly stratified sandstone	Pale grey	fU–mU (177 to 375); Moderate – well	Ungraded	No data	Isolated beds; proximal	Clay-poor sandstone can display crude tractional structures and elongate, sub-angular mud-clasts	Winnowed tractional deposits remnant from multiple episodes of bypass above an erosion surface (e.g. base of channel, scour or bedform trough)
Rb Deformed strata	–	–	–	No data	Anywhere but most common proximally	Sandstones or mudstones exhibit post-depositional soft (e.g. shear fold) to brittle (e.g. micro-faults) deformation structures. Often associated with variable scale ptygmatic sandstone dykes, lacking internal sedimentary structures. Present as units <1 m thick	Secondary deformation of sandstones and/or mudstones attributed to slumping and or sand remobilization and injection. Many are potential secondary slumps or debris flows triggered by incoming gravity currents (e.g. Stanley, 1982)
Mm Mudstone	Black – medium grey	Clay – Fine silt	–	No data	Inter bed; proximal–distal	Laminated to massive mudstone which ranges from highly to un-bioturbated	Hemipelagic suspension fallout from the water column

types draws from that of Lowe (1982), Haughton et al. (2009) and Baas et al. (2009), which outline flow behaviour largely according to sediment concentration and composition (i.e. non-cohesive versus cohesive, turbulent versus laminar, or flows with mixed behaviours).

Type A beds

Description: Very thin to medium-bedded (0·01 to 0·3 m thick), normally graded deposits of planar laminated and ripple cross-laminated sandstone (Ss, Table 1) with sharp, planar, non-erosive bed bases (Figs 5 and 6). Deposits are

Bed Type		Process interpretation	
A	**Bed thickness:** few cm to 30 cm. **Grain size:** silt to fine sand. **Sedimentary stuctures:** dominated by non-stratified matrix-poor sandstone (Sma) with subordinate stratified as, normally graded.	**Low-density non-cohesive turbulent flow**	Deposition and tractional working beneath a dilute low-density turbidity current (Lowe, 1982; Hiscott, 1994a).
B	**Bed thickness:** 20 to 110 cm. **Grain size:** fine to medium sand. **Sedimentary structures:** dominated by non-stratified matrix-poor sandstone (Sma) with subordinate stratified (Ss) or banded sandstone (Sb).	**High-density non-cohesive flow**	Largely deposited beneath high-density non-cohesive flow with high suspension fall out rates (*sensu* Lowe, 1982). Minor deposition from cohesive flow.
C	**Bed thickness:** 40 to 200 cm, **Grain size:** upper very fine to lower medium sand. **Sedimentary structures:** wide range of facies (Sma, Ss, Sb and Smu) with Sb thickness exceeding 30% of bed thickness and that of overlying facies Smu. Common dewatering structures. Mud-clast rich and mud-clast poor examples occur.	**Mixed non-cohesive and cohesive flow** Proximal	**Bed Type C:** Initial deposition from relatively non-cohesive flow (Sma and Ss). Significant deposition from near-bed flow that fluctuated between turbulent and relatively more cohesive states (Sb; Baas et al., 2005). Final deposition from cohesive quasi-laminar flow (Smu).
D	**Bed thickness:** 25 to 200 cm. **Grain size:** upper very fine to lower medium sand. **Sedimentary structures:** wide range of facies (Sma, Ss, Sb and Smu) with Smu thickness exceeding 30% of the bed thickness and that of underlying facies Sb. Mud-clast-rich and mud-clast poor examples.	Distal	**Bed Type D:** As for Type C beds. However, deposition beneath cohesive, quasi-laminar flow was more significant during later stages of deposition of the bed (Smu).
E	**Bed thickness:** 20 to 65 cm. **Grain size:** clay to fine sand. **Sedimentary structures:** facies Smu and Rb with poorly sorted, non-graded, plastic deformation fold and shear structures, weak to absent fabrics in mud-clasts.	**Cohesive quasi-laminar flow**	Cohesive, laminar debris flow deposition (Lowe, 1982; Sohn et al., 1997).

Planar lamination   Current-ripple lamination   Clasts   Dewatering   Banding
Turbulent   Laminar   Non-cohesive   Cohesive

Fig. 5. Descriptions and depositional process interpretations for discrete event beds found within sandstones of the Springar Formation.
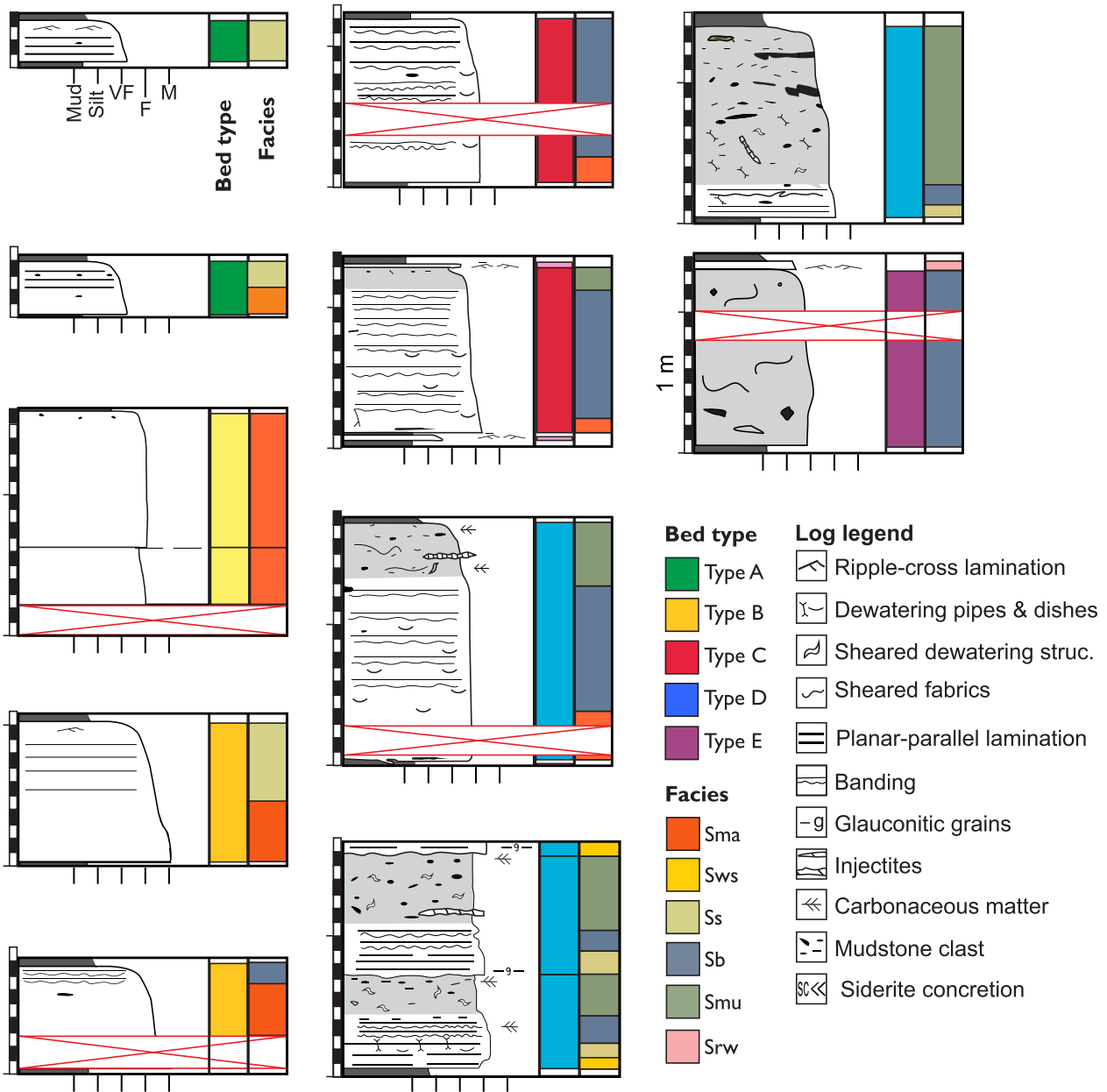
Fig. 6. Graphic sedimentary logs showing examples of common bed types found within the Lower Sandstone: VF = very fine sand; F = fine sand; M = medium sand.

typically mud-clast poor; where clasts are present they are typically several millimetres in length and are aligned along laminae.

Interpretation: Type A sediment gravity flow deposits were emplaced by dilute (low sediment concentration) turbulent suspensions, in which grain support by fluid-turbulence permitted differential-grain settling, bed traction and the development of associated sedimentation structures (e.g. low-density turbidity current, *sensu* Lowe, 1982; Bouma, 1962).

Type B beds

Description: Medium-bedded to very thick-bedded (0·2 to 1·1 m), normally graded deposits dominated by clay-poor non-stratified sandstone with moderate to poor sorting (Sma, Table 1, Figs 5 to 7). Non-stratified sandstone is overlain by thinner occurrences of planar laminated sandstone (Ss), or less commonly by banded sandstone (Sb). In the case of banded sandstone, it is the dominance of clay-poor non-stratified sandstone that distinguishes Type B beds from

Type C beds, which are instead dominated by banded sandstone. Bedding-aligned mud clasts (*ca* 0·01 m) and dewatering dishes can be present. Erosive bed bases occur and may exhibit sole structures.

Interpretation: Deposits dominated by clay-poor non-stratified sandstone with normal grading are attributed to progressive deposition beneath non-cohesive largely high-concentration flow, which underwent a decline in sediment concentration during late-stage deposition of stratified sandstone (i.e. high-density turbidity current, Lowe, 1982). Deposits that instead have thin occurrences of banded sandstone at the bed top imply that late-stage deposition occurred beneath fluctuating non-cohesive and cohesive behaviour (i.e. Lowe & Guy, 2000; Baas *et al.*, 2005). Such behaviour was probably promoted by a subtle increase in the proportion of clay within the flow (e.g. Baas & Best, 2002).

Type C and D beds

The type and arrangement of facies within Type C and D beds are similar, with the proportion of these facies being the major difference between the bed types. As such these bed types are described together and comparisons are made where pertinent, in order to gain insight into depositional processes and inferred flow behaviour.

Description: Type C and D beds typically comprise medium-bedded to very thick-bedded (0·25 to 2·0 m) deposits with weak normal grading and contain a wide range of facies types (Figs 5 and 6; Table 1). Where all facies are present, the deposits typically commence with clay-poor non-stratified sandstone (Sma) that is overlain by planar-laminated sandstone or weakly stratified sandstone (Ss and Sws), which are in turn overlain by banded sandstone (Sb) with clay-rich non-stratified sandstone at the bed top (Smu); capping laminated sandstones at the bed top are lacking (i.e. the H5 division of Haughton *et al.*, 2009). The bed top is overlain by mudstone, associated with background sedimentation, or is amalgamated with overlying beds. Facies contacts are largely gradational (over a few centimetres), with no dramatic change in grain size. Both erosive bed bases, sometimes with sole structures, and non-erosive bed bases are observed.

Type C and D beds exhibit an upward enrichment of detrital clay and other low-settling velocity particles (e.g. mica and plant fragments), and a subsequent decline in porosity and permeability (Figs 8 and 9). Banded sandstones often exhibit a saw-tooth mini-permeametry profile that reflects variations in the proportion of detrital clay between bands; higher permeability coincides with clay-poor bands. The decline in permeability is often greater than that of porosity due to the presence of micro-porosity in the clay-rich sandstone (e.g. Hurst & Nadeau, 1995). Note that poor reservoir quality can also occur lower within the bed (Sma, Ss and Sws) where preferential quartz cementation has occurred due to the lower proportion of detrital clay in these sandstones (Heald & Larese, 1974).
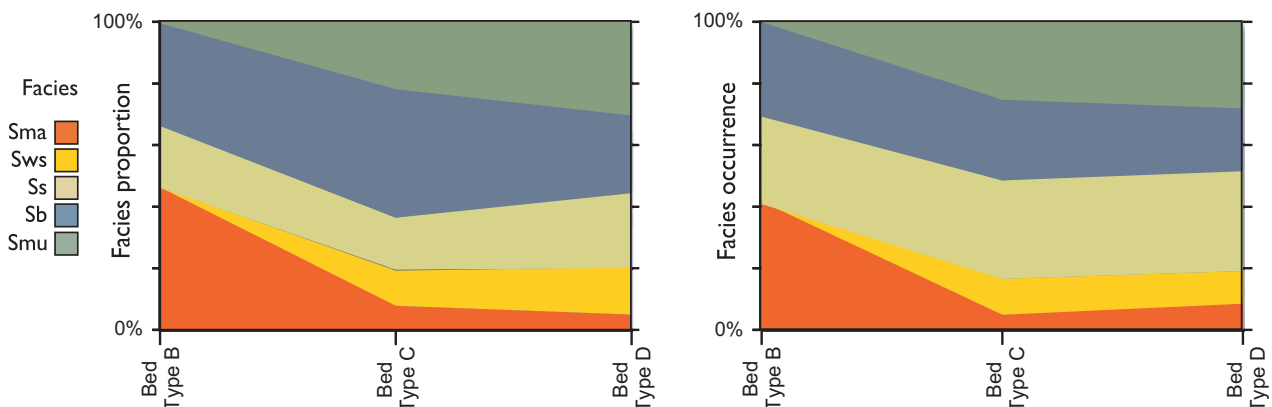
Fig. 7. Graphs depicting typical facies proportion (left) and facies occurrence (right) within bed types B, C and D. Determination of facies characteristics did not include beds affected by amalgamation or reworking at the bed top in order to avoid over-estimation of the thickness and occurrence of facies positioned lower within the bed.
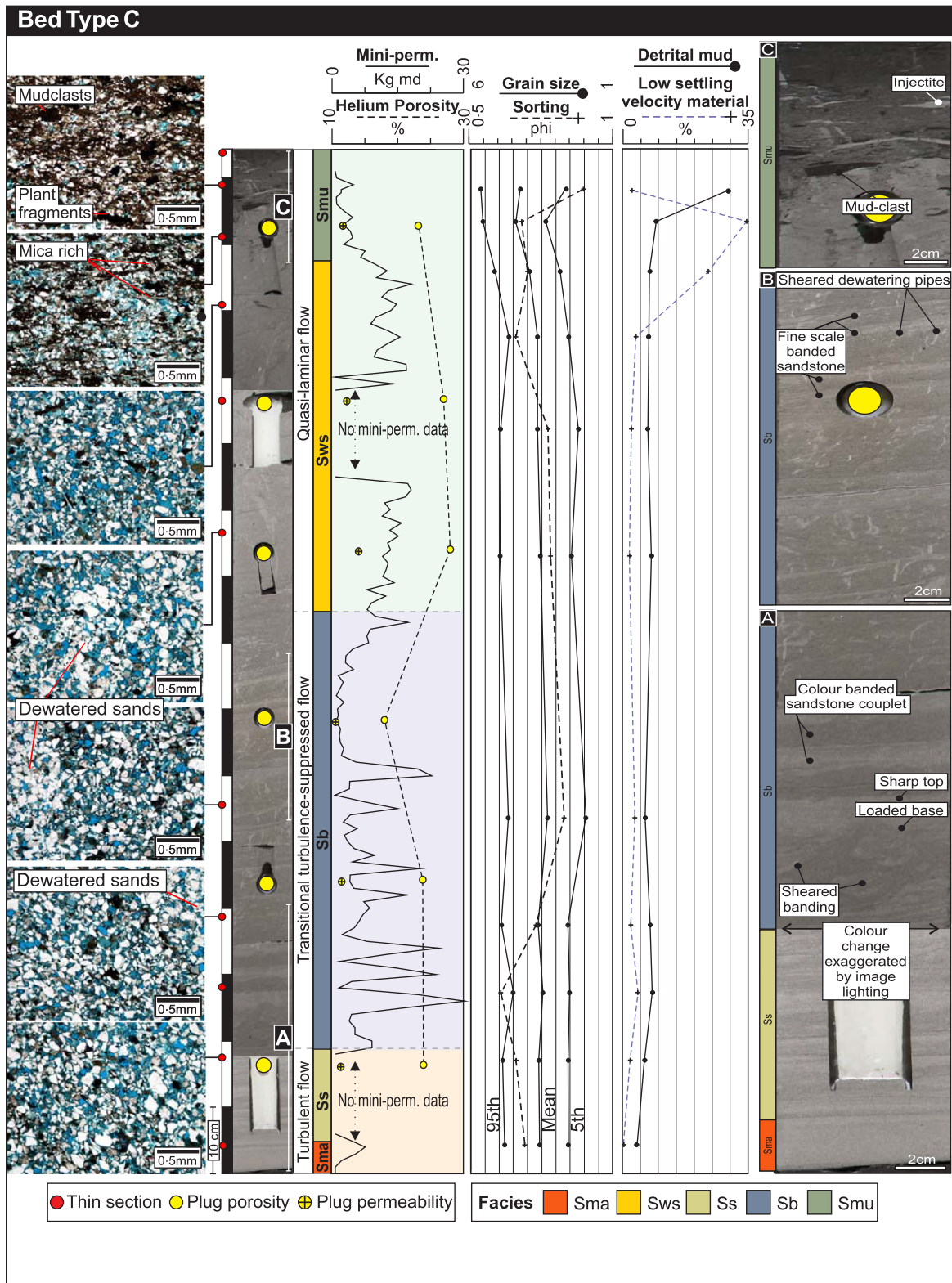
Fig. 8. Photographs of core and thin-sections (plane-polarized light) of a Type C bed dominated by banded sandstone (Sb). The vertical profile of the bed has been characterized in detail using mini-permeametry data (1 cm spacing), plug based helium porosity and permeability and point counting of thin-sections to determine grain size and sorting, as well as the proportion of detrital muds and other low-settling velocity material (carbonaceous material, mica grains and mud clasts). See text for description.
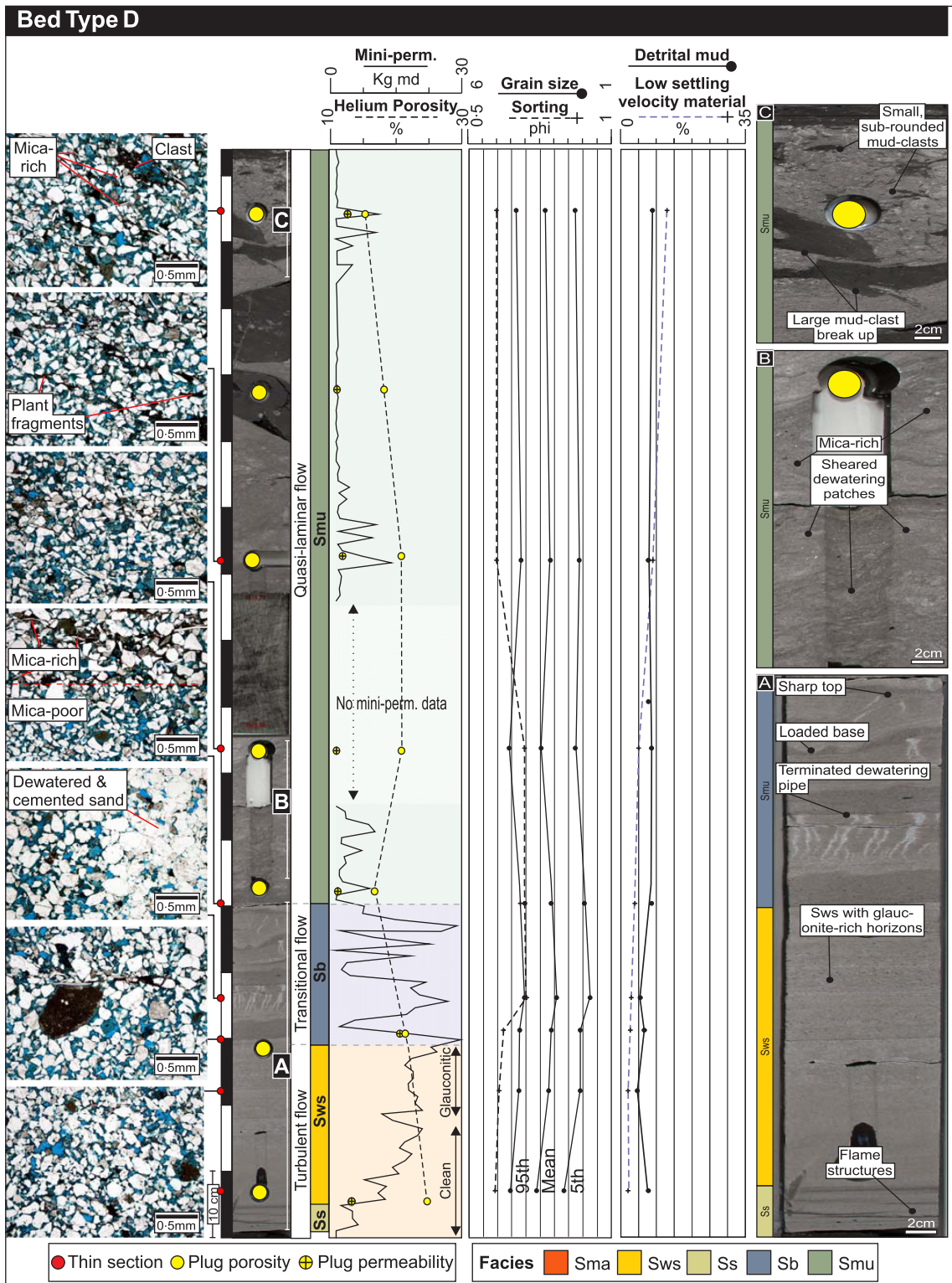
Fig. 9. Photographs of core and thin-sections (plane-polarized light) of a Type D bed dominated by highly argilla-ceous sandstone (Smu). The vertical profile of the bed has been characterized in detail using mini-permeametry data (1 cm spacing), plug based helium porosity and permeability and point counting of thin-sections to deter-mine grain size and sorting, as well as the proportion of detrital muds and other low-settling velocity material (carbonaceous material, mica grains and mud clasts). See text for description.

When compared with Type B beds, Type C and D beds show a significantly reduced occurrence and thickness of clay-poor non-stratified sandstone, in addition to increases in the occurrence and thickness of stratified sandstone and clay-rich non-stratified sandstone (Fig. 7). Type D beds are distinguished from Type C beds where the thickness of the clay-rich non-stratified sandstone exceeds that of banded sandstone. Occurrences of clay-poor non-stratified sandstone are thinner in Type D beds when compared with Type C beds (Fig. 7). Grain-size variation between Type C and D beds is not recognized due to the narrow grain-size range at any given well location.

Interpretation: The repeated association of clay-poor and overlying clay-rich sandstone facies without intervening mudstone has been documented in a number of studies, and implies that the facies are co-genetic in that they were deposited from a single sediment gravity flow (e.g. Lowe & Guy, 2000; Haughton *et al.*, 2003, 2009; Talling *et al.*, 2004; Barker *et al.*, 2008; Talling *et al.*, 2010; Kane & Pontén, 2012). Clay-poor non-stratified sandstone at the base of such deposits has previously been attributed to the following mechanisms: (i) deposition beneath a non-cohesive flow behaviour within a flow that exhibited spatial and temporal variation to more cohesive behaviour (i.e. Haughton *et al.*, 2003, 2009; Barker *et al.*, 2008); or (ii) late-stage sand settling from a cohesive sediment gravity flow in which the yield strength was insufficient to support the coarser sand fractions (Marr *et al.*, 2001; Talling *et al.*, 2010, 2012a,b; Type III experimental deposits of Sumner *et al.*, 2009).

A number of Type C and D bed characteristics are inconsistent with deposition via mechanism (ii) or by *en masse* flow freezing. Stratified and banded sandstones are a clear indicator of incremental aggradation of the bed beneath a passing sediment gravity flow (e.g. Allen, 1985; Lowe & Guy, 2000). It is difficult to envisage how a cohesive sediment gravity flow could be suitably stratified in terms of sediment composition, texture and subsequent rheology in order to produce the observed facies types and their vertical arrangement within Type C and D beds; such flows are not recognized in the laboratory or in nature. Furthermore, stratified sandstone specifically records deposition beneath dilute turbulent non-cohesive flow. Thus, the clay-poor non-stratified sandstone probably was deposited by similarly non-cohesive flow, albeit with higher sediment concentration, suspension fall-out and suppression of bed traction (Lowe, 1982).

The type and vertical arrangement of facies within Type C and D beds provides a temporal record of changing near-bed flow behaviour during the passing of a single sediment gravity flow, as observed at a fixed depositional point. Thus, Type C and D beds are interpreted as the depositional products of flow events that were characterized by longitudinal heterogeneity in the behaviour of near-bed flow (i.e. hybrid flow, *sensu* Haughton *et al.*, 2009). A non-cohesive (clay-poor) region at the front of the flow (i.e. Sma, Sws or Ss) was succeeded by a region that fluctuated between cohesive and non-cohesive behaviour (Sb), which was in turn followed by more stable cohesive flow behaviour in the rear of the flow (Smu). Type C and D beds are considered to have been emplaced by flows that were either: (i) the downstream continuation of flows emplacing Type B beds that had become clay-enriched (e.g. Amy & Talling, 2006; Fonnesu *et al.*, 2015); or (ii) separate flow events that were characterized by higher clay proportions (e.g. Lee *et al.*, 2013). Similar inferences can be made for Type D beds when compared with Type C beds, because thicker occurrences of clay-rich non-stratified sandstone suggest that more deposition occurred beneath a cohesive flow behaviour.

Type E beds

Description: Type E beds comprise thin to thick-bedded (0·20 to 0·65 m), non-graded deposits of clay-rich non-stratified poorly sorted sandstone (Smu) or deformed heterolithic strata (Rb, Figs 5 and 6). The clay-rich sandstone often has outsized sand grains and a 'starry night' appearance when compared with that in Type C and D beds (Smu, Table 1). Sub-angular to sub-rounded mud clasts, and rare sand clasts, are wide ranging in size and exhibit variable orientation to bedding. Bed bases are sharp and are planar or irregular.

Interpretation: Type E beds are interpreted as the products of slumps and cohesive, laminar debris flows (Lowe, 1982; Sohn *et al.*, 1997).

Type F beds

Description: Type F beds comprise thick-bedded (0·35 to 0·90 m), normally graded deposits of poorly sorted clay-poor non-stratified
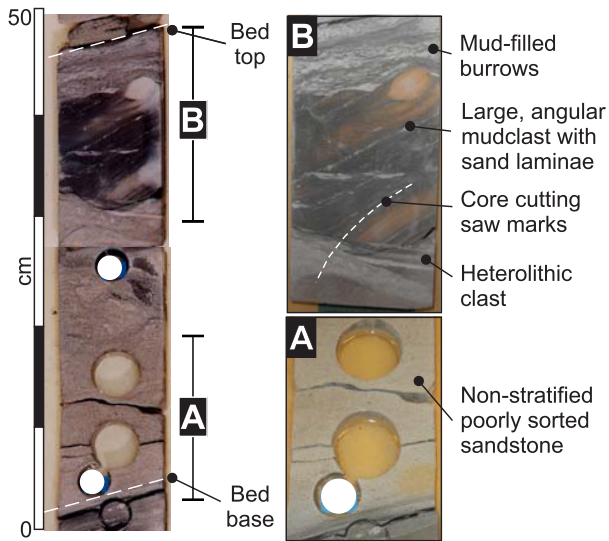
Fig. 10. Core photographs showing an example of the deposits found in Well 1; non-stratified sandstone (Sma) are directly overlain by clay-rich non-stratified sandstone containing large angular mud clasts.

sandstone (Sma), which are directly overlain by thinner occurrences of clay-rich non-stratified sandstone (Smu, Fig. 10). Type F beds lack occurrences of banded sandstone, which distinguishes them from Type C and D beds. Angular clasts of heterolithic strata can be larger than the 0·08 m width of the core. Bed bases are sharp, planar and may be erosive or non-erosive. Type F beds are only present in Well 1.

Interpretation: Type F beds are considered to be either a discrete type of hybrid flow that did not emplace banded sandstones (e.g. Haughton *et al.*, 2009; Talling, 2013), or composite deposits produced by sediment gravity flows that triggered destabilization of local sea-floor topography associated with the Gjallar Ridge (cf. Stanley, 1982; Kneller & McCaffrey, 1999). The latter could be implied by the abundance of larger, angular clasts and the proximity of Well 1 to the developing Gjallar Ridge. However, due to the limited core recovery from Well 1 the origin of Type F beds is ambiguous.

STRATIGRAPHIC AND SPATIAL VARIATION IN THE LOWER SANDSTONE

The Lower Sandstone (LS) accumulated during biozone 23.4, a period of *ca* 0·75 Myr (Fig. 2).
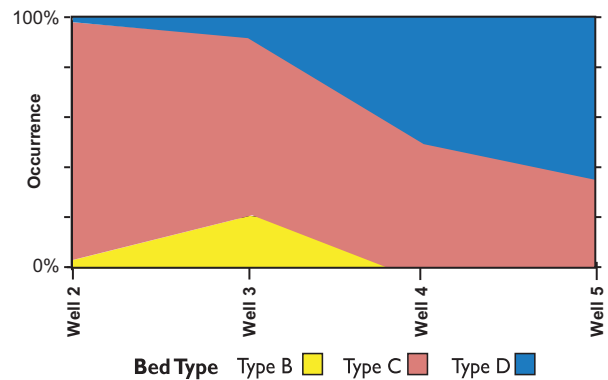

Fig. 11. Fence diagram depicting the distribution of key bed types B, C and D in the Lower Sandstone as observed in core from Wells 2 to 5. Type C beds are dominant in Wells 2 and 3, with subordinate Type D and B beds. Deeper in the basin at Wells 4 and 5, Type D beds are dominant, Type C beds become subordinate and Type B beds are entirely absent.

When compared with wells located relatively proximal to source, the LS in relatively distal wells 4 and 5 shows a reduction in the degree of bed amalgamation (*sensu* Romans *et al.*, 2009), sand to mud ratio, grain size and total thickness (Fig. 2). Type C and D beds are common within the LS and are most dominant in distal settings where Type B are absent (Fig. 11). Although partial core recovery can affect the absolute bed proportions documented, it is important to note the absence of Type B beds in distal wells; particularly in Well 4 where the LS was cored in full. Seismic amplitude extracts are generally of poor quality but appear to highlight weakly channelized sheets near Wells 2 and 3, with more lobate bodies occurring near Wells 4 and 5. The upper boundary of the LS exhibits an abrupt upward increase in gamma in all wells located downstream of the Gjallar Ridge (Wells 2 to 5), and records a sudden shut-down of sediment supply in the basin, as indicated by the thick mudstone-dominated succession in Well 1 (*ca* 2850 m, Fig. 2). The following sections provide brief descriptions and interpretations of sandstones from the five studied wells.

Well 1 – 6704/12-1

Well 1 represents the most proximal well in the regional context (Fig. 1). Here the LS consists of several mudstone-bound sandstone packages, and is parted from the Middle Sandstone by a *ca* 35 m thick, high-gamma

mudstone-dominated interval. The top of the Middle Sandstone is erosionally and unconformably overlain by Danian-aged strata (Fig. 2). The absence of the Upper Sandstone in Well 1 is attributed to continued uplift and erosion of the Gjallar Ridge (Roberts *et al.*, 1999). A limited amount of core (8·4 m) was recovered from the LS. It contains Type F beds along with deposits of complexly stratified sandstone (Srw) that display opposing current-direction indicators and internal scouring (Figs 3 and 10). The latter deposits record bottom current reworking (Lovell & Stow, 1981; Stow & Faugères, 2008), and may either directly overlie Type F beds or occur as isolated deposits bound by mudstones recording background sedimentation. Type F beds exhibit the coarsest grain sizes, yet the overall interval has low sand to mud and amalgamation ratios that are more comparable with those in Wells 4 to 5.

Interpretation: When compared with the LS penetrated in Wells 2 to 5, Well 1 may represent the off-axis or distal setting of a separate, yet more proximal to source, splay off of the main fairway (i.e. coarser grain sizes, relatively low sand to mud ratio and amalgamation ratio, occurrence upstream of the Gjallar Ridge). However, this is difficult to constrain considering the limited context and core recovery and, subsequently, Well 1 does not form a significant part of the analysis herein.

Well 2 – 6705/10-1

The LS sand (13·6 m) has a blocky gamma profile (Fig. 2) and commences with a thin deposit of facies St (0·03 m), which records local winnowing beneath gravity flows. This is overlain by a thick (13·5 m) succession of highly amalgamated Type C beds (Fig. 3). These beds are the dominant bed type (Fig. 11) and contain grain-size changes that delineate bedding contacts, as well as an abundance of dewatering structures (Fig. 3). Compared with Wells 3 to 5, the grain size, sand to mud ratio and amalgamation ratio are greater and grain sorting is poorer (Fig. 2).

Above the LS is a 4 m-thick interval where the biozone could not be determined; if biozones 23.2 to 23.3 are present within this interval then they exhibit a dramatic reduction in thickness at Well 2 (Figs 2 and 12). The interval commences with a 1 m-thick mudstone displaying lamination that is discordant to depositional

stratification with beds, bed tops and bases, and the top of the LS (Fig. 12); the lamination within the mudstone suggests that it is not *in situ*. The mudstone is overlain by deposits that contain a basal thin clay-poor sandstone, with an erosive base and angular rip-up clasts, which is directly overlain by mud-clast and clay-rich sandstone (Smu) or deformed strata (Rb). Above the 4 m-thick interval, the Upper Sandstone (biozone 23.1) comprises another thick succession of highly amalgamated and dewatered banded sandstones with bedding orientated similar to that in the LS (Fig. 2).

Interpretation: Well 2 is located more proximal to source compared to Wells 3 to 5 (e.g. thin facies St, coarser grain sizes, poorer sorting, higher bed amalgamation and sand to mud ratio). The LS is thought to have been penetrated in an off-axis position near the local base of slope of the Gjallar Ridge considering the degree of amalgamation, high sand to mud ratio and the lack of evidence for significant channelization (e.g. inclined erosional cuts, tractional lags and rip-up clasts). The repeated deposition of thick amalgamated dewatered banded sandstones in both the LS and Upper Sandstone record a significant amount of deposition beneath near-bed flow with transitional cohesive and non-cohesive behaviour (e.g. Baas *et al.*, 2005, 2011). Rapid deceleration of clay-rich flows has been shown to promote a change from non-cohesive to relatively more cohesive flow (cf. Baas *et al.*, 2009, 2011; Sumner *et al.*, 2009), a process that may have occurred on the downstream side of the developing Gjallar Ridge.

The 4 m-thick interval between the LS and the Upper Sandstone is interpreted to record remobilization and erosion processes due to a pulse of uplift in the Gjallar Ridge area. This would account for the limited thickness of the LS at Well 2. Furthermore, it could explain the missing or limited thickness of biozones 23.2 to 23.3, which were either deposited during a period of overall bypass or were removed by subsequent remobilization. Deposits containing rip-up clasts may be a direct result of such remobilization, and record a short-lived period of enhanced entrainment of mud-rich substrate during slope readjustment (cf. Haughton *et al.*, 2009). Deposition of the overlying Upper Sandstone may record erosion and reworking of sediment on the Gjallar Ridge; however, this cannot be constrained with the data available.
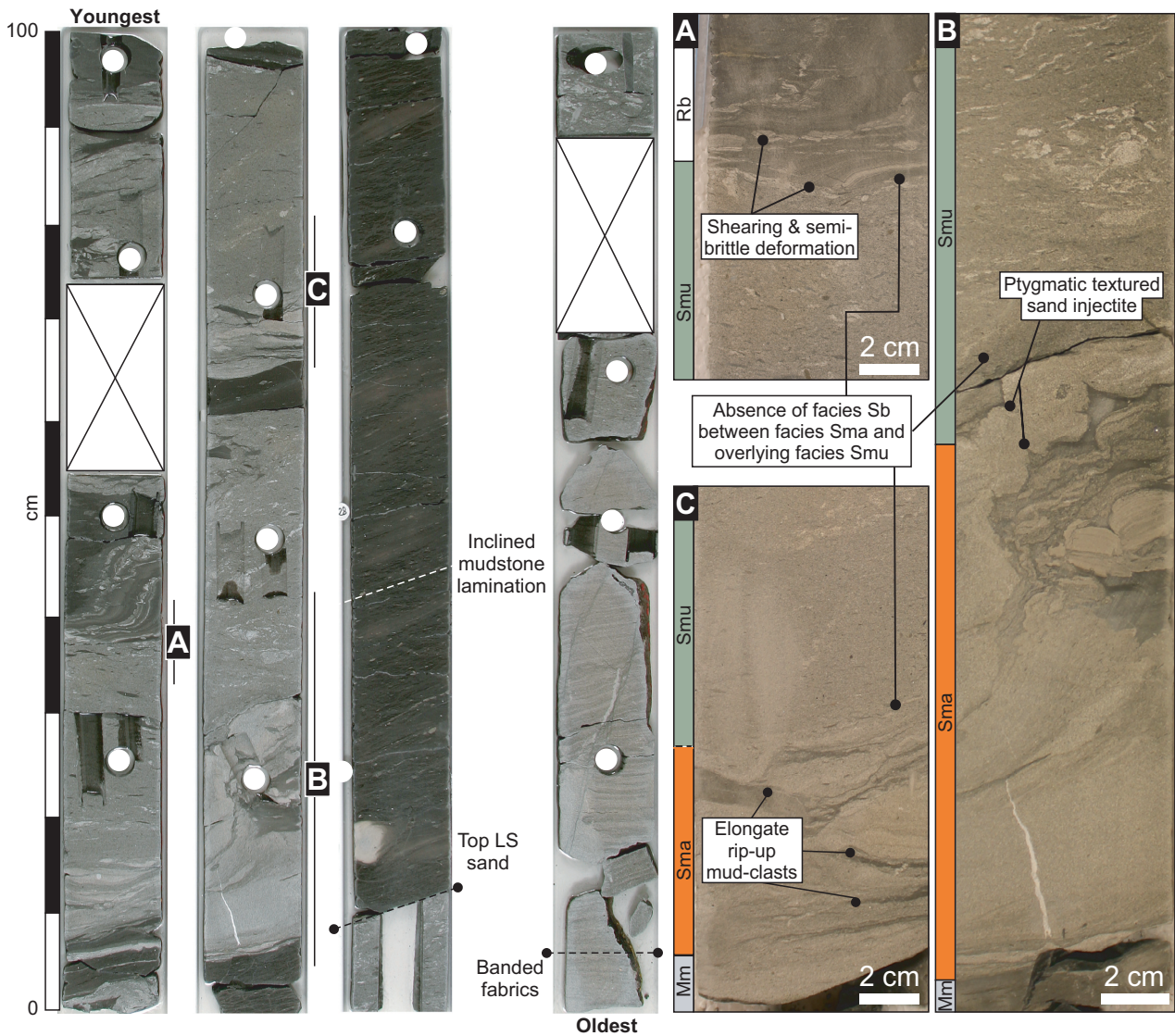
Fig. 12. Core photographs from Well 2 showing the interval of indeterminate biostratigraphy above the Lower Sandstone (LS). Laminations in the mudstone above the LS are inclined, suggesting that it is not in *in situ* (i.e. post-depositional remobilization). Overlying deposits comprise a basal relatively clay-poor sandstone (Sma), often containing rip-up clasts, which is directly overlain by non-stratified clay-rich sandstone (Smu) or slumped hetero-lithic strata (Rb); banded sandstones (Sb) are lacking from these deposits.

Well 3 – 6605/1-1

The LS at Well 3 has a greater total thickness (98·00 m) compared with that in Wells 4 and 5 (Fig. 2). The sand to mud ratio, amalgamation ratio, grain size and sorting of the cored interval (27·10 m) is intermediate between that observed in the more proximally located Well 2 and distally located Wells 4 and 5. The core exhibits a mixed succession of Type B and C beds, with a serrated gamma response, which is overlain by a Type C dominated package with comparatively lower gamma and a higher degree of

amalgamation (Figs 3 and 13). Type C beds are the most dominant at Well 3 (Fig. 11). The upper package shows an upward increase in gamma and a decrease in amalgamation; the lower package exhibits no vertical trend (Fig. 13). Overall, there is a vertical transition from Type B to Type C beds, with a thinning of non-stratified sandstone, thickening of banded sandstone and the appearance of clay-rich non-stratified sandstones (Fig. 13). Bed bases are commonly erosive; however features associated with sediment bypass are lacking (i.e. facies St
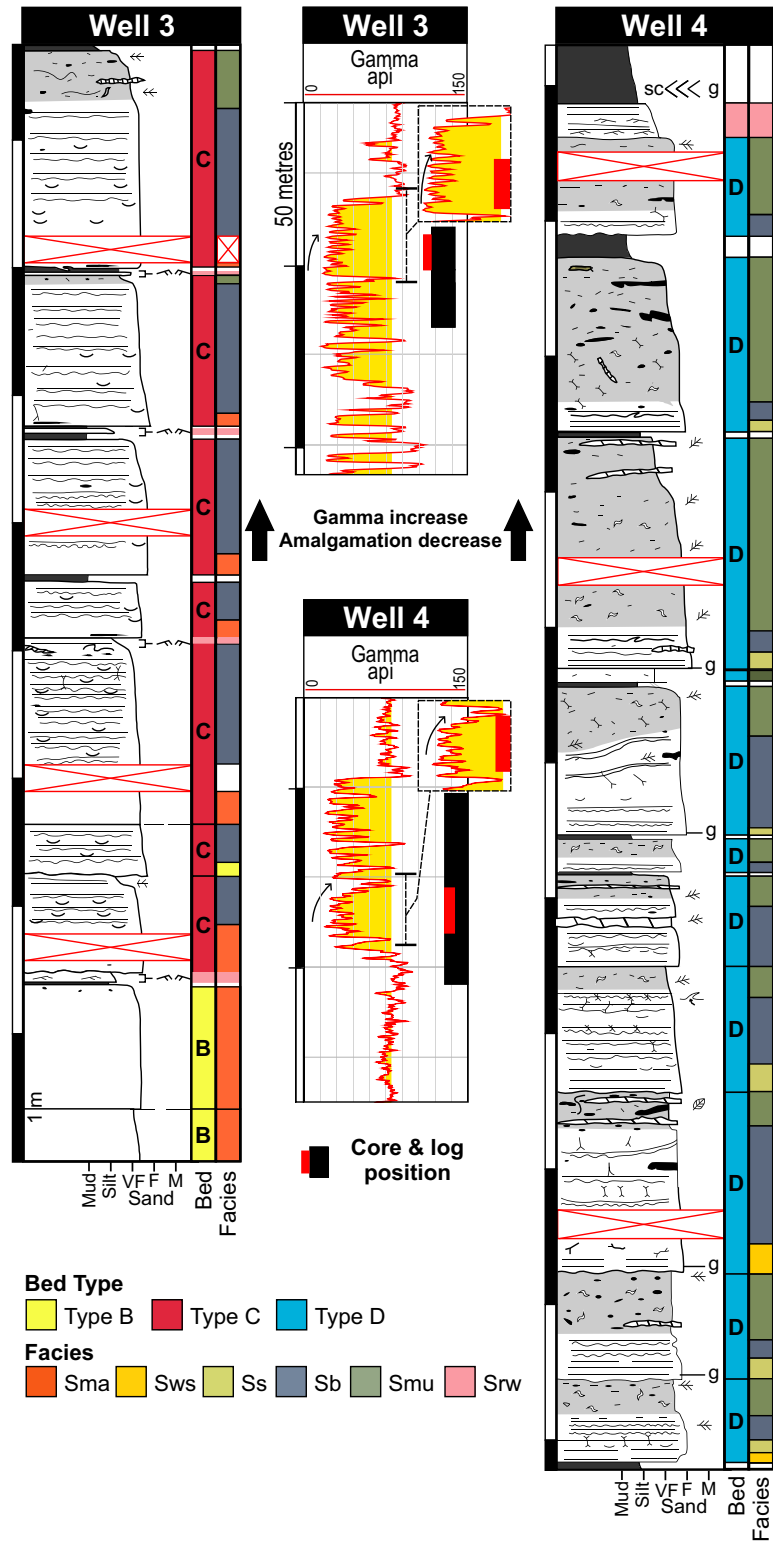
Fig. 13. Packages in Wells 3 and 4 exhibit an upward decrease in bed amalgamation and increase in gamma, with a capping condensed mudstone in Well 4, and are interpreted to record increasingly distal deposition prior to abandonment. In Well 3, as the bed type changes vertically from Type B to Type C, facies Sma exhibit a reduction in thickness whilst facies Smu thickness increases. In Well 4, stacked Type D beds exhibit an upward thinning of facies Sb and thickening of facies Smu. See Fig. 6 for the legend for graphic sedimentary logs: VF = very fine; F = fine; M = medium.

and rip-up mud clasts). The sand-rich interval is overlain by a mudstone containing a siderite concretion.

Interpretation: A moderate degree of amalgamation, high sand to mud ratio and a lack of evidence for significant channelization suggests

deposition in an off-axis position of a basin-floor fan, which was relatively distal from source compared to Well 2. The cored succession records an overall increase in the energy of subsequent flow events during deposition of the LS (e.g. increased amalgamation and sand to mud ratio) with a shift of deposition basinward or laterally promoting more axial deposition. On a smaller scale, the upper package captures an upward reduction in flow energy (landward or lateral shift to off-axis positions) during late-stage deposition of the LS, suggesting that Type C beds represent relatively more distal deposition compared to Type B beds (i.e. Walther's Law). The overlying mudstone with siderite concretions represents a condensed interval and limited sedimentation, at least locally (MacQuaker & Taylor, 1996).

Well 4 – 6604/10-1

The total thickness of the LS in Well 4 (55·20 m) is less than that in Well 3, and was largely captured by the cored interval (53·87 m, Figs 2 and 3). There is a progressive vertical decrease in gamma at the base of the LS, whereas the top of the LS is characterized by an abrupt increase in gamma (Fig. 2). The amalgamation ratio, sand to mud ratio, grain size and sorting are lower compared with Wells 2 and 3. The LS commences with a basal package that exhibits a progressive decrease then increase in gamma, which is overlain by three mudstone-bound packages that lack distinct trends in their gamma profiles (Fig. 2). The uppermost of these mudstone-bound packages is parted from the others by a notably thick (1·1 m) mudstone with high gamma. Features associated with significant sediment erosion or bypass are lacking (i.e. facies St and rip-up mud clasts) and bed bases are typically non-erosive. The dominant bed type in the LS changes vertically from Type A, through Type D to Type C. This is concomitant with an overall increase in the amalgamation and sand to mud ratios in successive packages (Figs 2 and 3).

In the basal package, the initial upward gamma decrease is driven by the change from thinner Type A beds to thicker Type D beds and an overall increase in bed amalgamation (Fig. 13). Change to upward decreasing gamma coincides with reduced bed amalgamation and thickening of clay-rich non-stratified sandstone within a succession of Type D beds. The LS is overlain by a mudstone with siderite concretions.

Interpretation: Well 4 is considered to penetrate the distal setting of a basin-floor fan (e.g. low amalgamation, low sand to mud ratio, reduced total thickness, finer grain sizes and limited evidence of erosion). An overall vertical increase in flow energy occurred during deposition of the LS (i.e. increased amalgamation and sand to mud ratios), which is similar to that in Well 3 and is interpreted to record a basinward or lateral shift to more axial deposition. Smaller-scale packages can record reductions in flow energy and increasingly distal deposition, with thickening of clay-rich non-stratified sandstone within Type D beds. The overlying mudstone with siderite concretions represents a condensed interval and limited sedimentation (MacQuaker & Taylor, 1996).

Well 5 – 6603/12-1

Well 5 contains the thinnest occurrence of the LS (35·00 m) with 18·47 m of core recovered and shares a number of similarities with Well 4 (Figs 2 and 3). The basal boundary also exhibits a progressive upward decrease in gamma, with a more abrupt gamma increase occurring at the top of the LS. A high-gamma mudstone (*ca* 1·40 m) also parts an upper package from the underlying lower packages. Vertically, the dominant bed type also changes from Type D to Type C beds (Fig. 3). The amalgamation ratio, sand to mud ratio, grain size and sorting are also comparable with those in Well 4 (Fig. 2).

Interpretation: The similarities between the core and gamma response, together with the biostratigraphic constraint and their close proximity (<10 km), suggests that Wells 4 and 5 penetrate the distal settings of the same lobe. The lower total thickness of the LS in Well 5 suggests that it is more distal or off-axis when compared with Well 4.

Spatial variation in facies within Type C and D beds

The characteristics of facies (occurrence and proportion) within Type C and D beds were determined at different wells (Fig. 14A). This approach was aimed at gaining insight into potential variations in depositional processes and inferred flow behaviour at different points in the basin; other bed types were not included due to their limited occurrence across the basin. Furthermore, beds affected by amalgamation were

excluded in order to avoid bias towards facies that are positioned lower within the bed, which are not affected by erosion at the bed top. Considering these criteria, Wells 1 and 2 are not examined in this analysis. For a given bed type, facies occurrence refers to how common a facies type is, whereas facies proportion refers to the typical thickness of a facies type; both are expressed as percentages. Facies characteristics were also determined specifically just for the facies type present at the base of Type C and D beds (Fig. 14B). This was aimed at gaining insight into variations in the depositional processes associated with the onset of deposition from the frontal regions of hybrid flows. Bed bases were easily identified by their contact with underlying mudstones, or by amalgamation surfaces that are delineated by grain-size changes.

Type C beds

The occurrence and proportion of both clay-poor non-stratified sandstone (facies Sma) and banded sandstone (facies Sb) decreases from Wells 3 to 5, whereas both stratified sandstone (facies Ss) and clay-rich non-stratified sandstone (facies Smu) exhibit an increase (Fig. 14A). Furthermore, the relative importance of facies Ss and Sma changes distally, with Ss becoming dominant in terms of proportion and occurrence in Wells 4 and 5. Similar variation is also observed for bed-basal facies, with higher occurrences and proportion of Sma in Well 3, and Ss in Wells 4 and 5 (Fig. 14B).

Type D beds

Facies characteristics were only determined at Wells 4 and 5 because non-amalgamated Type D beds are lacking at Well 3. From Wells 4 to 5 there is a decrease in the proportion of Sma and Sb, along with an increase in the proportion of Ss and Smu. In both Wells 4 and 5 there is a higher proportion of Ss when compared to Sma; this is true regardless of their position within the bed (Fig. 14A and B). Thus, facies characteristics in Type D beds are most comparable to Type C beds located in Wells 4 and 5, and exhibit similar spatial variation in facies characteristics to those that occur between Wells 3 to 5 in Type C beds (e.g. dominance of Ss relative to Sma, and thickening of Ss and Smu). However, when compared with Type C beds from the same well, the facies recording deposition with transient (Sb) or stable (Smu) cohesive flow behaviour are more significant in Type D beds (Fig. 15). Considering this, in addition to their

dominance in distal settings (Fig. 11), Type D beds are suggested to represent relatively clay-richer flow and more distal deposition.

DISCUSSION

Significance of variations documented within the Lower Sandstone

Building on the regional-scale setting (e.g. Lundin & Doré, 1997; Færseth & Lien, 2002; Roberts *et al.*, 2009), along with the interpretations of fan sub-environment for each well, Fig. 16 presents a conceptual model that summarizes the key aspects during deposition of the LS. Despite the general age-correlation of the LS, its exact stratigraphic correlation is subject to uncertainty (excluding Wells 4 to 5) due to the limitations of the seismic quality and lack of distinct lithological markers or high-resolution biostratigraphic data. Considering this, along with the spatial extent of the well transect (*ca* 140 km), it is unlikely that the documented variations in facies and bed type are a direct record of that which occurs across an individual lobe element or lobe; variations are instead more likely to capture regional-scale variation within a lobe complex (*sensu* Prélat *et al.*, 2009).

Sea-floor topography associated with the developing Gjallar Ridge is considered to have been a moderate influence upon deposition of the LS, because both Late Campanian and Maastrichtian strata exhibit local thinning towards the ridge (e.g. Bjørnseth *et al.*, 1997), and sandstones sourced from East Greenland extended deep into the basin (Morton *et al.*, 2005). Well 1 is located upstream of the Gjallar Ridge and is dominated by Type F deposits that record either: (i) deposition from discrete hybrid flows in the distal or off-axis parts of a lobe that was relatively more proximal to source; or (ii) gravity-current triggered destabilization of local sea-floor topography (cf. Stanley, 1982). The low amalgamation ratio and sand to mud ratio may favour the latter; however, it is difficult to discount either mechanism considering the limited amount of core recovered. The repetitive successions of highly amalgamated, dewatered banded sandstone in Well 2 are thought to record the local influence and overprinting effect of sea-floor topography associated with proximity to the Gjallar Ridge base of slope (Figs 2 and 3). It is thought that the local rapid deceleration of clay-rich flow promoted increased sediment
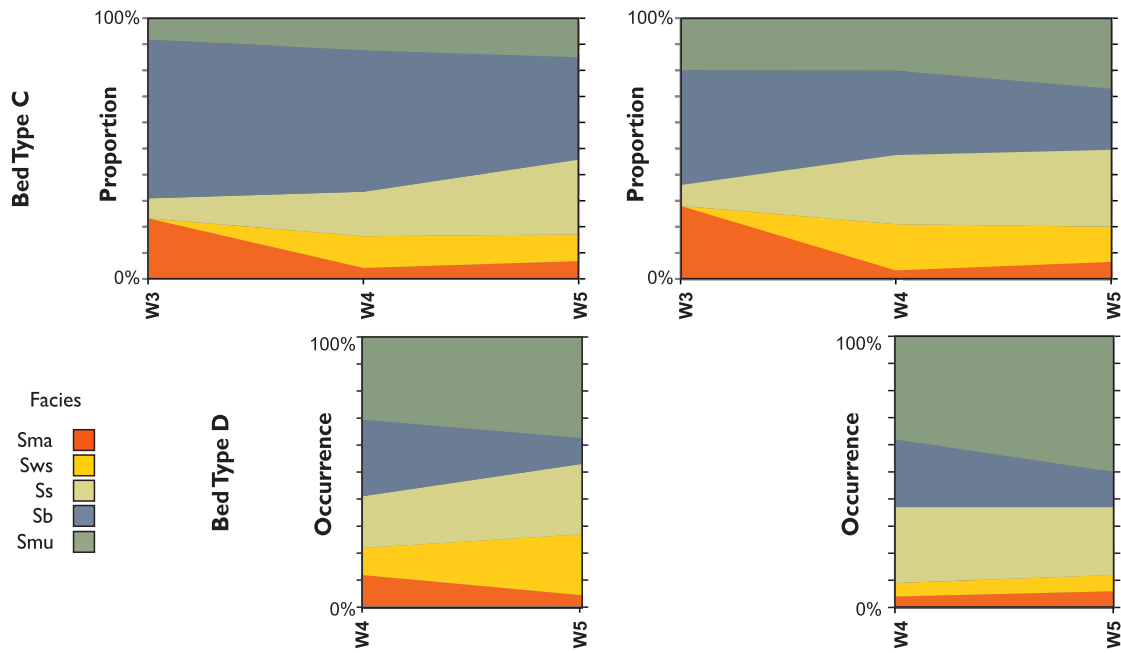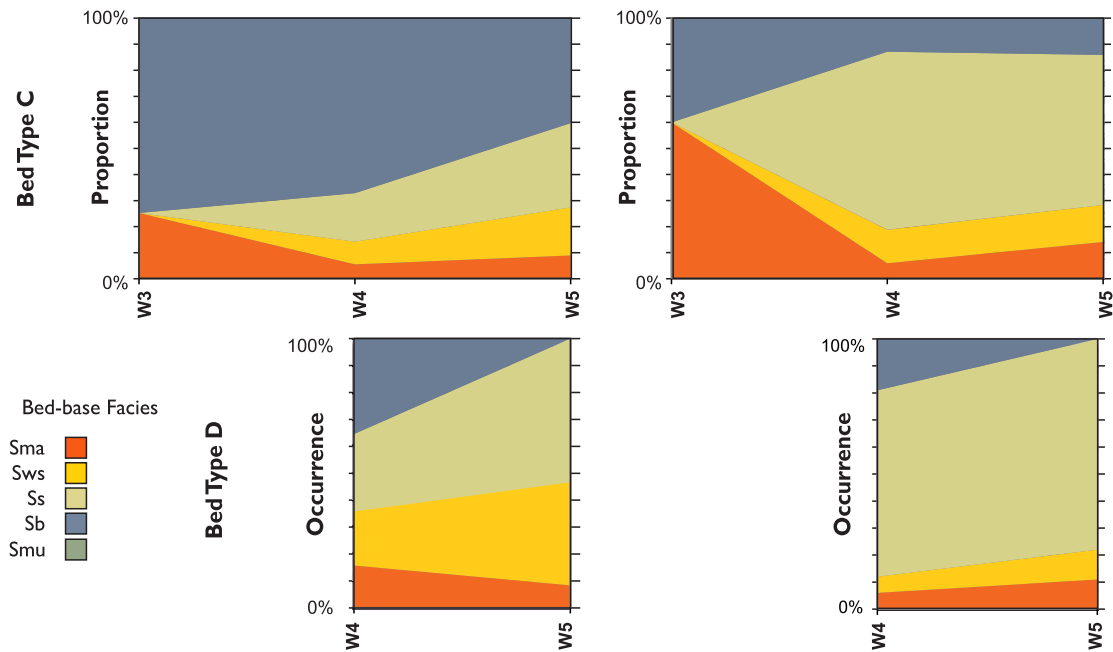
Fig. 14. (A) Fence diagrams illustrating variations in the proportion and occurrence of facies at Wells 3, 4 and 5 for Type C and D beds. (B) As for (A), but only facies present at the very base of the bed are considered. Beds with amalgamated or reworked tops were excluded to avoid over-estimation of characteristics for facies lower in the bed.

concentration and reduced fluid turbulence (cf. Lowe, 1975; Vrolijk & Southard, 1997), with a subsequent reduction in the flow Reynolds number and onset of more cohesive flow behaviour (Talling *et al.*, 2007; Barker *et al.*, 2008). Such changes may have only occurred in the

Fig. 15. Fence diagram comparing the proportion of facies deposited beneath cohesive flow (Sb and Smu) and non-cohesive flow (Sma, Ss and Sws) in Type C and D beds at Wells 4 (left) and 5 (right).

depositional boundary layer due to settling of sediment into a dense near-bed flow layer. Although banded sandstone can be deposited in the absence of sea-floor topography (e.g. Haughton *et al.*, 2009), comparable thicknesses of banded sandstone within hybrid event beds

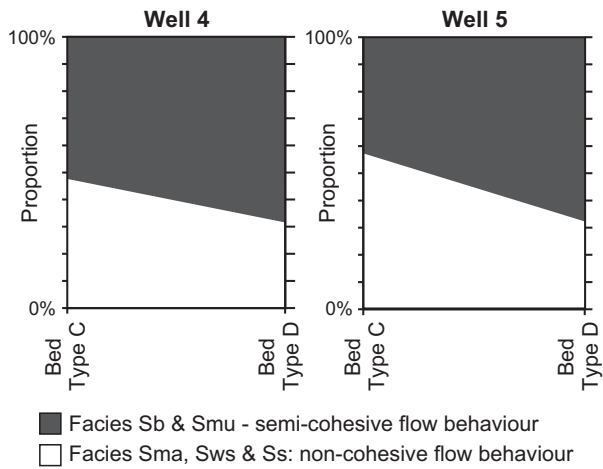have only been documented in the Britannia Sandstone, North Sea (Blackbourn & Thomson, 2000; Lowe & Guy, 2000; Barker *et al.*, 2008); a system where sea-floor topography is also thought to have influenced depositional facies (Barker *et al.*, 2008). The near exclusive dominance of banded sandstone in the LS at Well 2 at least suggests there was a sustained, perhaps local, influence upon deposition.

Increasingly distal styles of deposition occur deeper in the basin (e.g. decreased amalgamation ratio, sand to mud ratio, grain size, total thickness and increased sorting). The local reduced thickness of the LS at Well 2 is attributed to post-depositional erosion following continued uplift of the Gjallar Ridge. Concomitant with these basinward changes is an increase in the occurrence of hybrid event beds (Type C and D) and loss of Type B beds, with a notable increase in the occurrence of Type D beds that record more cohesive flow behaviour and more distal deposition (Fig. 11). Continued uplift of the Gjallar Ridge is thought to have reduced the sediment supply deeper in the basin (i.e. absence of Middle Sandstone in Wells 2 to 5). Deposition of the Upper Sandstone either records a fairway that exploited a low point in
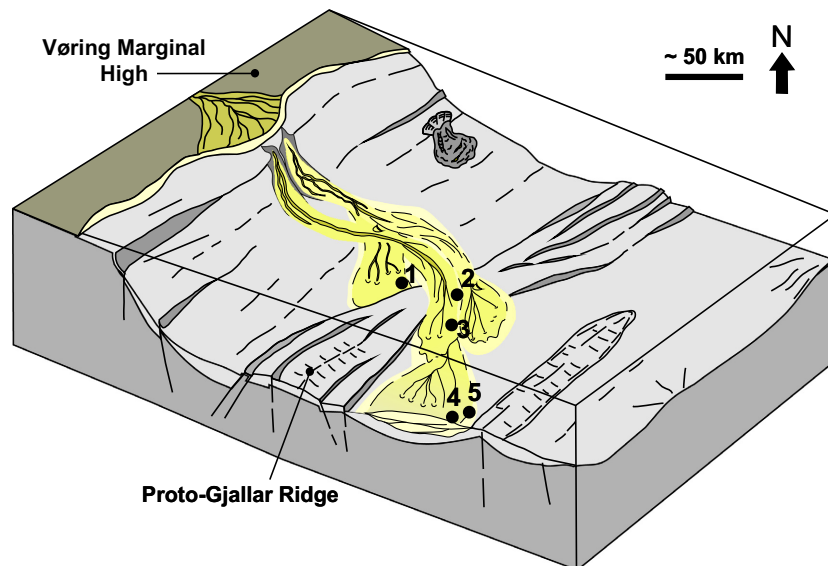
Fig. 16. Conceptual block diagram depicting the main features and aspects of sedimentation within the northwest Vøring Basin during emplacement of the Lower Sandstone (LS). Well penetrations are tentatively assigned to sub-environments of the fan model based on core descriptions and wireline responses; seismic data does not provide a strong constraint on these depositional environments. The developing Gjallar Ridge was dissected by north-west/south-east trending lineaments that permitted deposition deeper in the basin (Fjellanger *et al.*, 2005). The position of the shelf is poorly constrained, but is approximated by the eastern limit of the Vøring Marginal High (Roberts *et al.*, 1997; Færseth & Lien, 2002).

the ridge, or local erosion and resedimentation from the Gjallar Ridge.

Process model for deposits comprising co-genetic clay-poor and clay-rich sandstone

Based on the observed variation in bed type and facies characteristics within the LS, Fig. 17 presents a conceptual process model that depicts inferred downstream changes in the longitudinal structure of near-bed flow within hybrid flows. Although the variations captured by Wells 2 to 5 may represent relatively proximal and distal parts of separate sedimentary bodies, they are still thought to provide insight into the variations in flow character that can occur with differing flow run-out distances and variable interaction with local sea-floor topography.

Overall, the longitudinal structure of near-bed flow behaviour became increasingly heterogeneous during downstream run-out, as zones of transitional (facies Sb) and cohesive quasi-laminar turbulence-suppressed (Smu) flow behaviour were developed in the rear of the flow (i.e. hybrid flow, *sensu* Haughton *et al.*, 2009). Comparable flow evolution has been documented in a number of studies and is attributed to the enrichment of clay within flows either by: (i) entrainment of muddy substrate (Haughton *et al.*, 2003, 2009); or (ii) deceleration and deposition of coarser sand fractions (Talling *et al.*, 2004, 2007; Sumner *et al.*, 2009). Initiation of a cohesive behaviour is most likely to occur in the clay-rich rear of flows that are characterized by longitudinal variations in grain size and composition (i.e. Baas *et al.*, 2005, 2011). Initially, transitional flow was most dominant in hybrid flows and deposited the thick banded sandstone in Type C beds. With increasing flow run-out distance and clay-enrichment, the region of steadier quasi-laminar cohesive flow became increasingly significant in the rear of hybrid flows (i.e. facies Smu, Type D beds); enhancement of this flow state may drive the distal reduction in banded sandstone thickness as rearward regions of near-bed flow became clay-enriched (Fig. 11). Concomitantly, the front of the hybrid flow remained non-cohesive and underwent a discrete style of evolution, presumably in response to deposition and declining sediment concentration (Fig. 17). The front of the hybrid flow evolved from flow with a high sediment concentration and suspension fall-out rate with capacity-driven deposition (i.e. basal occurrences of Sma), to flow behaviour that became increasingly dilute and turbulent with competence-driven deposition (i.e. basal occurrences of Ss). Such non-cohesive flow and its downstream variation suggests that hybrid flows in the LS most probably evolved from non-cohesive sediment gravity flows, rather than by dilution or acceleration of cohesive flows (i.e. Talling *et al.*, 2007). The described variations in flow behaviour could occur either during the downstream run-out of individual sediment gravity flows that were prone to clay-enrichment and the development of longitudinally heterogeneous near-bed flow (i.e. Fig 17), or in separate flow events with increasing proportions of clay.

Comparisons with other models

The observations and interpretations presented herein are aligned with many current models that concern hybrid event bed and transitional flow deposit distribution within deep-water depositional systems (e.g. Haughton *et al.*, 2003, 2009; Talling *et al.*, 2004, 2012a; Amy & Talling, 2006; Barker *et al.*, 2008; Hodgson, 2009; Kane & Pontén, 2012). This study provides further insight into the flow processes associated with the emplacement of these deposit types.

Thickness of banded sandstones
The position of banded sandstone between underlying clay-poor sandstone facies and overlying clay-rich sandstone facies is similar to that observed in hybrid event beds from other deep-water systems (Lowe & Guy, 2000; Haughton *et al.*, 2003, 2009; Barker *et al.*, 2008; Sylvester & Lowe, 2004). However, the proportion of banded sandstone is significantly greater than that documented in most of these studies, with the exception of the Cretaceous Britannia Sandstone, North Sea (Lowe & Guy, 2000; Barker *et al.*, 2008). As discussed previously, it is inferred here that rapid deceleration of clay-rich flows near the Gjallar Ridge base of slope reduced turbulent kinetic energy and may have promoted the onset of more cohesive flow behaviour. Similarly, deposition of the Britannia Sandstone was associated with large-volume flows that healed and interacted with significant sea-floor topography associated with mass-transport deposits (Barker *et al.*, 2008; Eggenhuisen *et al.*, 2010). Thus, it is possible that thick occurrences of banded sandstone can be promoted by the interaction of clay-rich sediment gravity flows with pronounced or persistent sea-floor topography.
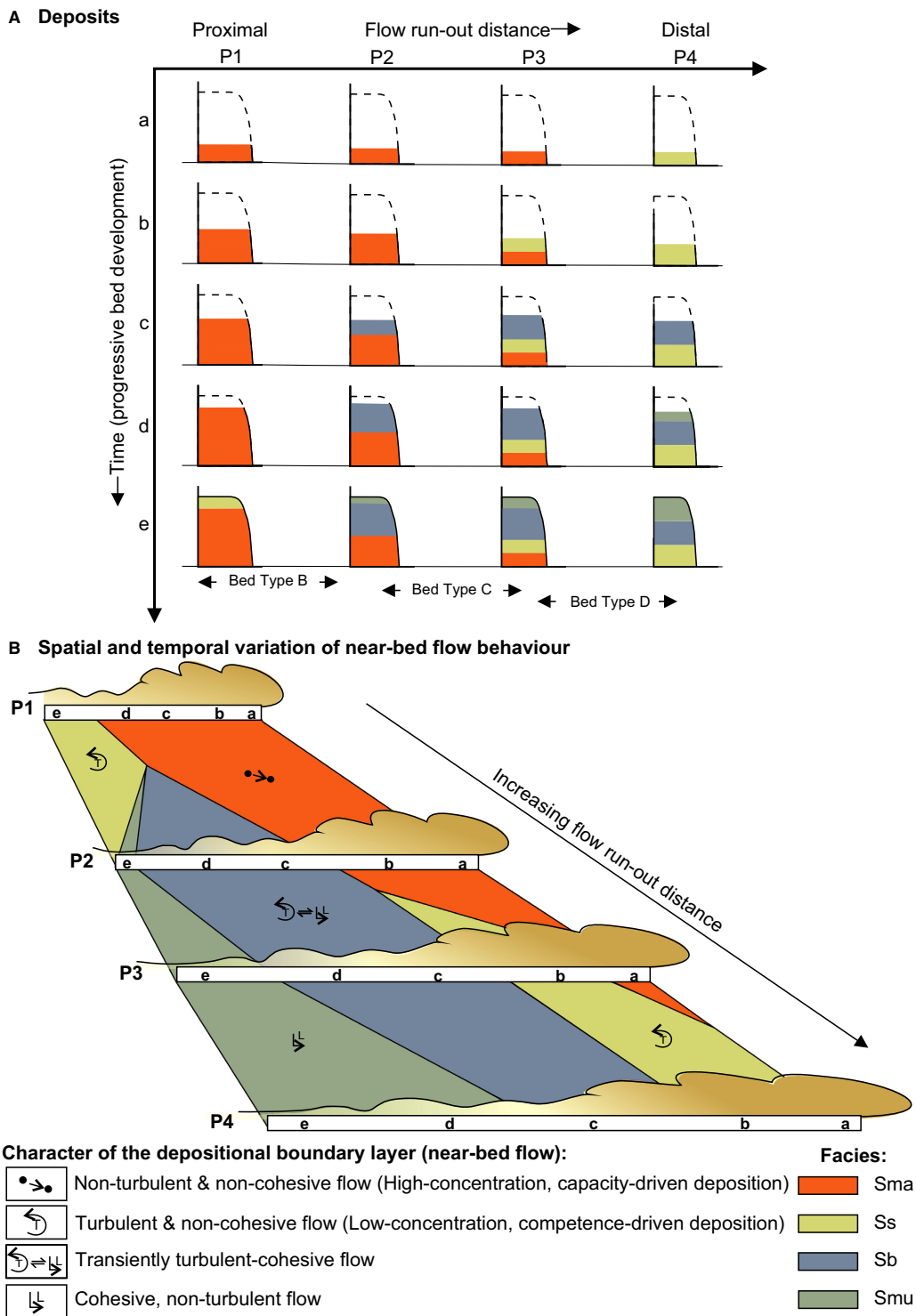
Fig. 17. Conceptual process model illustrating deposit accumulation (A) and inferred variation in near-bed flow character (B) at increasingly distal positions along the flow pathway. During flow run-out the character of near-bed flow evolves and becomes increasingly heterogeneous along the length of the flow ('a' to 'e'). The presence and relative importance of discrete rheological zones, and associated depositional facies, evolves due to variations in sediment concentration or the proportion of cohesive material within the flow. Frontal regions of the flow become increasingly turbulent as sediment concentration declines, whereas more rearward regions of the flow become increasingly turbulence-suppressed and cohesive due to increase in the proportion of clay and flow deceleration.

Significance of basal facies trends in beds containing co-genetic clay-poor and clay-rich sandstone

Non-stratified and stratified sandstones have been documented at the base of hybrid event beds and transitional deposits (Haughton *et al.*, 2003; Amy & Talling, 2006; Talling *et al.*, 2007; Barker *et al.*, 2008; Hodgson, 2009; Kane & Pontén, 2012). Individual beds in the Marnoso-Arenacea Formation have been correlated over distances of tens of kilometres, and provide the first documentation of downstream changes between non-stratified and stratified clay-poor sandstone at the base of hybrid event beds (Amy & Talling, 2006). However, to date, no studies have discussed the implications of this downstream facies change in terms of the behaviour and evolution of hybrid flows. The occurrence of this bed-base facies trend, both in this study (Fig. 14) and in the Marnoso-Arenacea Formation, suggests that the front of hybrid flows can remain non-cohesive and undergo a discrete style of evolution compared to the rear of the flow. Frontal regions of hybrid flow evolved from high-concentration turbulence-suppressed flow with capacity-driven deposition, to low-concentration turbulent flow with competence-driven deposition (Fig. 17); presumably in response to increasing deposition and declining sediment concentration during downstream run-out (Lowe, 1988; Mutti, 1992). Such non-cohesive flow and its downstream variation suggest that hybrid flows in the LS most probably evolved from non-cohesive sediment gravity flows, rather than by dilution or acceleration of cohesive flows (i.e. Talling *et al.*, 2007).

Kane & Pontén (2012) used repeated vertical stacking patterns in the Wilcox Formation, Gulf of Mexico, to infer downstream facies tracts that also record deposition beneath increasingly cohesive flow behaviour. The downstream transformation was attributed to the rapid deceleration of clay-rich flows upon exiting the channel mouth. Interestingly these authors documented a different bed-basal facies tract, with stratified sandstones being replaced by non-stratified sandstone downstream. We suggest that this reflects the mechanism by which the basal clay-poor sandstone was emplaced; Kane & Pontén (2012) propose emplacement of the non-stratified sandstone by sand settling through high-concentration quasi-cohesive flow (cf. Sumner *et al.*, 2009). Thus, their documented bed-basal facies tract records a different style of flow evolution, whereby flow emplacing the relatively clay-poor sandstone became increasingly turbulence-suppressed. As such, spatial variation in the relative importance of stratified and non-stratified clay-poor sandstone at the base of hybrid event beds are proposed to differ depending on the mechanism by which they are emplaced (i.e. beneath non-cohesive flow or via sand-settling from non-cohesive flow).

The implications of such variation in flow behaviour at the front of flow events that emplace co-genetic clay-poor and clay-rich sandstone are significant. Previous studies have shown how changes in sediment concentration, turbulent state and sedimentation rate influence flow interaction with the ambient fluid (e.g. Allen, 1985; Kneller & Buckee, 2000), the sea-floor substrate (Verhagen *et al.*, 2013; Baas *et al.*, 2014) and subsequent depositional character.

Reservoir implications

The clay-rich sandstone facies (Sb and Smu) are generally of poor-reservoir quality, and whilst they may contribute to overall recoverable volume and hydrocarbon drive, they are not worthwhile targets alone. The recognition that up-dip deposits contain thick proportions of banded sandstone (i.e. Wells 2 and 3), suggests that exploration further down-dip in the same system may encounter thick clay-rich non-stratified sandstones and would be ill advised. Similarly, the dominance of stratified sandstone at the base of hybrid event beds could be used as an indicator of relatively more distal settings, where clay-rich facies are greater in occurrence and proportion, and that exploration up-dip would be more preferable.

Limitations of analysing stratigraphic packages

Because the correlation of individual beds is generally not possible in subsurface data, this study uses stratigraphic packages correlated between wells to infer flow processes. As noted above, this approach runs the risk that beds representing different and independent downstream processes of flow evolution may be analysed jointly. Furthermore, given the constraints of seismic resolution, paucity of distinct lithological markers and lack of sufficiently high-resolution biostratigraphic data, the possibility that the LS represents separate fans of differing extent, rather than a single fan, cannot be eliminated. Subsequently there could either be: (i) hybrid flows in which the frontal non-

cohesive region of flow evolved from high to low-sediment concentration during downstream run-out, with concomitant change in the near-bed flow behaviour from turbulence-suppressed to turbulent; or (ii) a discrete class of hybrid flow that was always dilute and turbulent in the head, but typically bypassed proximal areas in favour of deposition in the most distal settings. Regardless, observations from hybrid event beds in relatively proximal and distal positions highlight the variation in flow properties that can occur at the front of hybrid flows. Despite the limitations of analysing stratigraphic packages in this context, a number of useful insights and models for predicting flow behaviour have been developed (e.g. Lowe & Guy, 2000; Lowe *et al.*, 2003; Haughton *et al.*, 2003, 2009; Barker *et al.*, 2008; Davis *et al.*, 2009). Given the paucity of outcrops where models for flow evolution can be reliably tested it is hoped that the observations here, along with detailed coring studies of the modern sea floor (e.g. Stevenson *et al.*, 2013; Talling *et al.*, 2015), will provide a framework for future physical and numerical modelling studies.

CONCLUSIONS

The range in the depositional character of hybrid event beds is inferred to reflect the complexity of flow transformation in sedimentary systems which are controlled by a complex interplay of allogenic and autogenic controls. An examination of the spatial and stratigraphic distribution of bed types, and the facies within hybrid event beds has highlighted the following:

1 The development of hybrid flows with longitudinally distributed discrete zones of flow behaviour (i.e. non-cohesive versus cohesive, turbulent versus turbulent-suppressed) within near-bed flow and variation in their relative importance in proximal and distal settings.
2 Rearward regions of near-bed flow in hybrid flows became increasingly clay-rich and turbulence-suppressed in distal settings, promoting deposition of banded and clay-rich non-stratified sandstones.
3 Frontal regions of near-bed flow remained clay-poor and non-cohesive, but underwent a decrease in sediment concentration and sediment fall-out rate that drove an increase in fluid turbulence, bed traction and relative importance of

stratified sandstone at the base of hybrid event beds compared to non-stratified sandstone.
4 Thus, hybrid flows are complex in that they can evolve both spatially and temporally with discrete, potentially simultaneous, styles of variation occurring in different regions of the flow event or between separate flow events.
5 Sediment gravity flows may have been primed for transformation to increasingly cohesive flow behaviour following deceleration at the Gjallar Ridge base of slope; prior to which significant entrainment of muddy substrate may have occurred above this ridge.
6 Thick occurrences of banded sandstone appear to be promoted by the interaction of clay-rich sediment gravity flows with persistent sea-floor topography (i.e. spatial decelerations).
7 The complex and dynamic nature of downstream flow evolution within sediment gravity flows that exhibit both cohesive and non-cohesive flow behaviour.

REFERENCES

Allen, J.R.L. (1984) Parallel lamination developed from upper-strage plane beds: a model based on the larger coherent structures of the turbulent boundary layer. *Sediment. Geol.*, **39**, 227–242.
Allen, J.R.L. (1985) *Principles of Physical Sedimentology.* George Allen & Unwin Ltd, London, 272 pp.
Allen, J.R.L. (1991) The Bouma A division and the possible duration of turbidity currents. *J. Sed. Res.*, **61**, 291–295.
Amy, L.A. and **Talling, P.J.** (2006) Anatomy of turbidites and linked debrites based on long distance (120 x 30 km) bed correlation, Marnoso Arenacea Formation, Northern Apennines, Italy. *Sedimentology*, **53**, 161–212.

Arnott, R.W.C. and **Hand, B.M.** (1989) Bedforms, primary structures and grain fabric in the presence of suspended sediment rain. *J. Sed. Res.*, **59**, 1062–1069.

Baas, J.H. and **Best, J.L.** (2002) Turbulence modulation in clay-rich sediment-laden flows and some implications for sediment deposition. *J. Sed. Res.*, **72**, 336–340.

Baas, J.H., **McCaffrey, W.D.**, **Haughton, P.D.W.** and **Choux, C.** (2005) Coupling between suspended sediment distribution and turbulence structure in a laboratory turbidity current. *J. Geophys. Res. Oceans*, **110**, 1–22.

Baas, J.H., **Best, J.L.**, **Peakall, J.** and **Wang, M.** (2009) A phase diagram for turbulent, transitional and laminar clay suspension flows. *J. Sed. Res.*, **79**, 162–183.

Baas, J.H., **Best, J.L.** and **Peakall, J.** (2011) Depositional processes, bed form development and hybrid bed formation in rapidly decelerated cohesive (mud–sand) sediment flows. *Sedimentology*, **58**, 1953–1987.

Baas, J.H., **Manica, R..**, **Puhl, E.**, **Verhagen, I.** and **O.Borges, A.L.** (2014) Processes and products of turbidity currents entering soft muddy substrates. *Geology*, **42**, 371–374.

Barker, S.P., **Haughton, P.D.W.**, **McCaffrey, W.D.**, **Archer, S.G.** and **Hakes, B.** (2008) Development of rheological heterogeneity in clay-rich high-density turbidity currents: Aptian Britannia Sandstone Member, UK continental shelf. *J. Sed. Res.*, **78**, 45–68.

Best, J. and **Bridge, J.** (1992) The morphology and dynamics of low amplitude bed-waves upon upper stage plane beds and the preservation of planar laminae. *Sedimentology*, **39**, 737–752.

Bjørnseth, H.M., **Grant, S.M.**, **Hansen, E.K.**, **Hossack, J.R.**, **Roberts, D.G.** and **Thompson, M.** (1997) Structural evolution of the Vøring Basin, Norway, during the Late Cretaceous and Palaeogene. *J. Geol. Soc.*, **154**, 559–563.

Blackbourn, G.A. and **Thomson, M.E.** (2000) Britannia Field, UK North Sea: petrographic constraints on Lower Cretaceous provenance, facies and the origin of slurry-flow deposits. *Petrol. Geosci.*, **6**, 329–343.

Bouma, A.H. (1962) *Sedimentology of Some Flysch Deposits: A Graphic Approach to Facies Interpretations*. Elsevier, Amsterdam, 168 pp.

Davis, C., **Haughton, P.D.W.**, **McCaffrey, W.D.**, **Scott, E.**, **Hogg, N.** and **Kitching, D.** (2009) Character and distribution of hybrid sediment gravity flow deposits from the outer Forties Fan, Palaeocene Central North Sea, UKCS. *Mar. Petrol. Geol.*, **26**, 1919–1939.

Eggenhuisen, J.T., **McCaffrey, W.D.**, **Haughton, P.D.W.**, **Butler, R.W.H.** and **Moore, I.** (2010) Reconstructing large-scale remobilisation of deep-water deposits and its impact on sand-body architecture from cored wells: the Lower Cretaceous Britannia Sandstone Formation, UK North Sea. *Mar. Petrol. Geol.*, **27**, 1595–1615.

Færseth, R. and **Lien, T.** (2002) Cretaceous evolution in the Norwegian Sea – a period characterised by tectonic quiescence. *Mar. Petrol. Geol.*, **19**, 1005–1027.

Fjellanger, E., **Sulryk, F.**, **Wamsteeker, L.C.** and **Midtun, T.** (2005) Upper Cretaceous basin-floor fans in the Vøring Basin, Mid Norway shelf. *Norwegian Petroleum Society Special Publications*, **12**(135), 164.

Fonneland, H.C., **Lien, T.**, **Martinsen, O.J.**, **Pedersen, R.B.** and **Kosler, J.** (2004) Detrital zircon ages: a key to understanding deposition of deep marine sandstones in the Norwegian Sea. *Sed. Geol.*, **164**, 147–159.

Fonnesu, M., **Haughton, P.**, **Felletti, F.** and **McCaffrey, W.** (2015) Short length-scale variability of hybrid event beds and its applied significance. *Mar. Petrol. Geol.*, **67**, 583–603.

Haughton, P.D.W., **Barker, S.P.** and **McCaffrey, W.D.** (2003) 'Linked' debrites in sand-rich turbidite systems – origin and significance. *Sedimentology*, **50**, 459–482.

Haughton, P.D.W., **Davis, C.**, **McCaffrey, W.D.** and **Barker, S.** (2009) Hybrid sediment gravity flow deposits – classification, origin and significance. *Mar. Petrol. Geol.*, **26**, 1900–1918.

Heald, M.T. and **Larese, R.E.** (1974) Influence of coatings on quartz cementation. *J. Sed. Res.*, **44**, 1269–1274.

Hodgson, D.M. (2009) Distribution and origin of hybrid beds in sand-rich submarine fans of the Tanqua depocentre, Karoo Basin, South Africa. *Mar. Petrol. Geol.*, **26**, 1940–1956.

Hubert, J.F. (1964) Textural evidence for deposition of many western North Atlantic deep-sea sands by ocean-bottom currents rather than turbidity currents. *Geology*, **72**, 757–785.

Hurst, A. and **Nadeau, P.H.** (1995) Clay micro-porosity in reservoir sandstones: an application of quantitative electron microscopy in petrophysical evaluation. *AAPG Bull.*, **79**, 563–573.

Kane, I.A. and **Pontén, A.S.M.** (2012) Submarine transitional flow deposits in the Paleogene Gulf of Mexico. *Geology*, **40**, 1119–1122.

Kittilsen, J.E., **Olsen, R.R.**, **Marten, R.F.**, **Hansen, E.K.** and **Hollingsworth, R.R.** (1999) The first deepwater well in Norway and its implications for the Upper Cretaceous Play, Voring Basin. In: *Petroleum Geology of Northwest Europe: Proceedings of the 5th Conference* (Eds A.J. Fleet and S.A.R. Boldy), pp. 275–280. The Geological Society, London.

Kneller, B.C. and **Branney, M.J.** (1995) Sustained high-density turbidity currents and the deposition of thick massive sands. *Sedimentology*, **42**, 607–616.

Kneller, B.C. and **Buckee, C.** (2000) The structure and fluid mechanics of turbidity currents: a review of some recent studies and their geological implications. *Sedimentology*, **47**, 62–94.

Kneller, B.C. and **McCaffrey, W.D.** (1999) Depositional effects of flow non-uniformity and stratification within turbidity currents approaching a bounding slope: deflection, reflection, and facies variation. *J. Sed. Res.*, **69**, 980–991.

Lee, S.H., **Jung, W.Y.**, **Bahk, J.J.**, **Gardner, J.M.**, **Kim, J.K.** and **Lee, S.H.** (2013) Depositional features of co-genetic turbidite–debrite beds and possible mechanisms for their formation in distal lobated bodies beyond the base-of-slope, Ulleung Basin, East Sea (Japan Sea). *Mar. Geol.*, **346**, 124–140.

Lien, T., **Midtbø, R.E.** and **Martinsen, O.J.** (2006) Depositional facies and reservoir quality of deep-marine sandstones in the Norwegian Sea. *Norw. J. Geol.*, **86**, 71–92.

Lovell, J.P.B. and **Stow, D.A.V.** (1981) Identification of ancient sandy contourites. *Geology*, **9**, 347–349.

Lowe, D.R. (1975) Water escape structures in coarse-grained sediment. *Sedimentology*, **46**, 157–204.

Lowe, D.R. (1982) Sediment gravity flows: II, depositional models with special reference to the deposits of high-density turbidity currents. *J. Sed. Res.*, **52**, 279–298.

Lowe, D.R. (1988) Suspended-load fallout rate as an independent variable in the analysis of current structures. *Sedimentology*, **35**, 765–776.

Lowe, D.R. and **Guy, M.** (2000) Slurry-flow deposits in the Britannia Formation (Lower Cretaceous), North Sea: a new perspective on the turbidity current and debris flow problem. *Sedimentology*, **47**, 31–70.

Lowe, D.R., **Guy, M.** and **Palfrey, A.** (2003) Facies of slurry-flow deposits, Britannia Formation (Lower Cretaceous), North Sea: implications for flow evolution and deposit geometry. *Sedimentology*, **50**, 45–80.

Lundin, E.R. and **Doré, A.G.** (1997) A tectonic model for the Norwegian passive margin with implications for the NE Atlantic: Early Cretaceous to break-up. *J. Geol. Soc. London*, **154**, 545–550.

Lundin, E.R., **Doré, A.G.**, **Rønning, K.** and **Kyrkjebø, R.** (2013) Repeated inversion and collapse in the Late Cretaceous-Cenozoic northern Vøring Basin, offshore Norway. *Petrol. Geosci.*, **19**, 329–341.

MacQuaker, J.H.S. and **Taylor, K.G.** (1996) A sequence-stratigraphic interpretation of a mudstone dominated succession: the Lower Jurassic Cleveland Ironstone Formation, UK. *J. Geol. Soc. London*, **153**, 759–770.

Major, J.J. (1997) Depositional processes in large-scale debris-flow experiments. *Geology*, **105**, 345–366.

Manica, R. (2012). Sediment gravity flows: study based on experimental simulations. In: *Hydrodynamics: Natural Water Bodies* (Eds H. Schulz, A. Simoes and R. Lobosco), pp. 263–286. InTech, Rijeka, Croatia.

Marr, J.G., **Harff, P.A.**, **Shanmugam, G.** and **Parker, G.** (2001) Experiments on subaqueous sandy gravity flows: the role of clay and water content in flow dynamics and depositional structures. *Geol. Soc. Am. Bull.*, **113**, 1377–1386.

Middleton, G.V. (1967) Experiments on density and turbidity currents: III. Deposition of sediment. *Can. J. Earth Sci.*, **4**, 475–505.

Mohrig, D. and **Marr, J.G.** (2003) Constraining the efficiency of turbidity current generation from submarine debris flows and slides using laboratory experiments. *Mar. Petrol. Geol.*, **20**, 883–899.

Morton, A.C., **Whitham, A.G.**, **Fanning, C.M.** and **Claoue-Long, J.** (2005) The role of East Greenland as a source of sediment to the Voring Basin during the Late Cretaceous. *Norw. Petrol. Soc. Spec. Publ.*, **12**, 83–110.

Mulder, T. and **Alexander, J.** (2001) The physical character of subaqueous sedimentary density flows and their deposits. *Sedimentology*, **48**, 269–299.

Mutti, E. (1992) Turbidite Sandstones. Istituto di Geologia Università di Parma, 275 pp.

Porten, K.W., **Kane, I.A.**, **Warchoł, M.J.** and **Southern, S.J.** (2016) A sedimentological process-based approach to depositional reservoir quality of deep-marine sand-stones: an example from the Springar Formation, north-western Vøring Basin, Norwegian Sea. *J. Sed. Res.*, **18**, 1–18.

Prélat, A., **Hodgson, D.M.** and **Flint, S.S.** (2009) Evolution, architecture and hierarchy of distributary deep-water deposits: a high-resolution outcrop investigation from the Permian Karoo Basin, South Africa. *Sedimentology*, **27**, 241–270.

Ricci Lucchi, F.R. and **Valmori, E.** (1980) Basin-wide turbidites in a Miocene, over-supplied deep-sea plain: a geometrical analysis. *Sedimentology*, **27**, 241–270.

Riis, F. (1996) Quantification of Cenozoic vertical movements on Scandinavia by correlation of morphological surfaces with offshore data. *Global Planet. Change*, **12**, 331–357.

Roberts, A.M., **Lundin, E.R.** and **Kusznir, N.J.** (1997) Subsidence of the Voring Basin and the influence of the Atlantic continental margin. *J. Geol. Soc. London*, **154**, 551–557.

Roberts, D.G., **Thompson, M.**, **Mitchener, B.**, **Hossack, J.**, **Carmichael, S.** and **Bjørnseth, H.M.** (1999) Palaeozoic to Tertiary rift and basin dynamics: mid-Norway to the Bay of Biscay–a new context for hydrocarbon prospectivity in the deep water frontier. In: *Petroleum Geology of Northwest Europe: Proceedings of the 5th Conference* (Eds A.J. Fleet and S.A.R. Boldy), pp. 7–40. The Geological Society, London.

Roberts, A.M., **Corfield, R.I.**, **Kusznir, N.J.**, **Matthews, S.J.**, **Hansen, E.K.** and **Hooper, R.J.** (2009) Mapping palaeostructure and palaeobathymetry along the Norwegian Atlantic continental margin: Møre and Vøring basins. *Petrol. Geosci.*, **15**, 27–43.

Romans, B.W., **Hubbard, S.M.** and **Graham, S.A.** (2009) Stratigraphic evolution of an outcropping continental slope system, Tres Pasos Formation at Cerro Divisadero, Chile. *Sedimentology*, **56**, 737–764.

Sanders, J.E. (1965) Primary sedimentary structures formed by turbidity currents and related resedimentation mechanisms. In: *Primary Sedimentary Structures and Their Hydrodynamic Interpretation* (Ed. G.V. Middleton), *SEPM Spec. Publ.*, **12**, 192–219.

Skogseid, J. and **Eldholm, O.** (1989) Voring continental margin: seismic interpretation, stratigraphy and vertical movements. In: *Proc. ODP Sci Results* (Eds O. Eldholm, J. Thiede and E. Taylor), *Ocean Drilling Program*, **104**, 993–1030.

Sohn, Y.K., **Kim, S.B.**, **Hwang, I.G.**, **Bahk, J.J.**, **Choe, M.Y.** and **Chough, S.K.** (1997) Characteristics and depositional processes of large-scale gravely gilbert-type forests in the Miocene Doumsan fan delta, Pohang Basin, SE Korea. *J. Sed. Res.*, **67**, 130–141.

Stanley, D.J. (1982) Welded slump-graded sand couplets: evidence for slide generated turbidity currents. *Geo-Mar. Lett.*, **2**, 149–155.

Stevenson, C.J., **Talling, P.J.**, **Wynn, R.B.**, **Masson, D.G.**, **Hunt, J.E.**, **Frenz, M.**, **Akhmetzhanhov, A.** and **Cronin, B.T.** (2013) The flows that left no trace: very large-volume turbidity currents that bypassed sediment through submarine channels without eroding the sea floor. *Mar. Petrol. Geol*, **41**, 186–205.

Stevenson, C.J., **Talling, P.**, **Masson, D.G.**, **Sumner, E.J.**, **Frenz, M.** and **Wynn, R.B.** (2014) The spatial and temporal distribution of grain-size breaks in turbidites. *Sedimentology*, **61**, 1120–1156.

Stow, D.A.V. and **Faugères, J.C.** (2008) Contourite facies and the facies model. *Dev. Sedimentol.*, **60**, 223–256.

Stow, D.A.V., **Reading, H.G.** and **Collinson, J.D.** (1996) Deep seas. In: *Sedimentary Environments: Processes, Facies and Stratigraphy* (Ed. H.G. Reading), pp. 395–453. Blackwell Science, Oxford.

Sumner, E.J., **Talling, P.J.** and **Amy, L.A.** (2009) Deposits of flows transitional between turbidity current and debris flow. *Geology*, **37**, 991–994.

Surlyk, F. (1990) Timing, style and sedimentary evolution of Late Palaeozoic-Mesozoic extensional basins of East Greenland. *Geol. Soc. London. Spec. Publ.*, **55**, 107–125.

Sylvester, Z. and **Lowe, D.R.** (2004) Textural trends in turbidites and slurry beds from the Oligocene flysch of the East Carpathians, Romania. *Sedimentology*, **51**, 945–972.

Talling, P.J. (2013) Hybrid submarine flows comprising turbidity current and cohesive debris flow: deposits,

theoretical and experimental analyses, and generalised models. *Geosphere*, **9**, 460–488.

Talling, P.J., **Amy, L.A.**, **Wynn, R.B.**, **Peakall, J.** and **Robinson, M.** (2004) Beds comprising debrite sandwiched within co-genetic turbidite: origin and widespread occurrence in distal depositional environments. *Sedimentology*, **51**, 163–194.

Talling, P.J., **Wynn, R.B.**, **Masson, D.G.**, **Frenz, M.**, **Cronin, B.T.**, **Schiebel, R.**, **Akhmetzhanov, A.M.**, **Dallmeier-Tiessen, S.**, **Benetti, S.**, **Weaver, P.P.E.**, **Georgiopoulou, A.**, **Zühlsdorff, C.** and **Amy, L.A.** (2007) Onset of submarine debris flow deposition far from original giant landslide. *Nature*, **450**, 541–544.

Talling, P.J., **Wynn, R.B.**, **Schmmidt, D.N.**, **Rixton, R.**, **Sumner, E.** and **Amy, L.** (2010) How did thin submarine debris flows carry Boulder-sized intraclasts for remarkable distances across low gradients to the far reaches of the Mississippi fan? *J. Sed. Res.*, **80**, 829–851.

Talling, P.J., **Malgesini, G.**, **Sumner, E.J.**, **Amy, L.A.**, **Felletti, F.**, **Blackbourn, G.**, **Nutt, C.**, **Wilcox, C.**, **Harding, I.C.** and **Khan, S.** (2012a) Planform geometry, stacking pattern, and extra-basinal origin of low-strength and intermediate-strength cohesive debris flow deposits in the Marnoso-arenacea Formation. *Geosphere*, **8**, 1–24.

Talling, P.J., **Masson, D.G.**, **Sumner, E.J.** and **Malgesini, G.** (2012b) Subaqueous sediment density flows: depositional processes and deposit types. *Sedimentology*, **59**, 1937–2003.

Talling, P.J., **Allin, J.**, **Armitage, D.A.**, **Arnott, R.W.C.**, **Cartigny, M.J.B.**, **Clare, M.A.**, **Felletti, F.**, **Covault, J.A.**, **Girardclos, S.**, **Hansen, E.**, **Hill, P.R.**, **Hiscott, R.N.**, **Hogg, A.J.**, **Clarke, J.H.**, **Jobe, Z.R.**, **Malgesini, G.**, **Mozzato, A.**, **Naruse, H.**, **Parkinson, S.**, **Peel, F.J.**, **Piper, D.J.W.**, **Pope, E.**, **Postma, G.**, **Rowley, P.**, **Sguazzini, A.**, **Stevenson, C.J.**, **Sumner, E.J.**, **Sylvester, Z.**, **Watts, C.** and **Xu, J.P.** (2015) Key future directions for research on turbidity currents and their deposits. *J. Sed. Res.*, **85**, 153–169.

Terlaky, V. and **Arnott, R.W.C.** (2014) Matrix-rich and associated matrix-poor sandstones: avulsion splays in slope and basin-floor strata. *Sedimentology*, **61**, 1175–1197.

Verhagen, I.T.E., **Baas, J.H.**, **Jacinto, R.S.**, **McCaffrey, W.D.** and **Davies, A.G.** (2013) A first classification scheme of flow-bed interaction for clay-laden density currents and soft substrates. *Ocean Dyn.*, **63**, 385–397.

Vrolijk, P.J. and **Southard, J.B.** (1997) Experiments on rapid deposition of sand from high-velocity flows. *Geosci. Can.*, **24**, 45–54.

Wood, A. and **Smith, A.J.** (1958) The sedimentation and sedimentary history of the Aberystwyth Grits (Upper Llandoverian). *J. Geol. Soc. London*, **114**, 163–195.